



**HAL**  
open science

## Implementation of an end-to-end model of the Gulf of Lions ecosystem (NW Mediterranean Sea). I. Parameterization, calibration and evaluation

Daniela Bănaru, Frederic Diaz, Philippe Verley, Rose Campbell, Jonathan Navarro, Christophe Yohia, Ricardo Oliveros-Ramos, Capucine Mellon-Duval, Yunne-Jai Shin

### ► To cite this version:

Daniela Bănaru, Frederic Diaz, Philippe Verley, Rose Campbell, Jonathan Navarro, et al.. Implementation of an end-to-end model of the Gulf of Lions ecosystem (NW Mediterranean Sea). I. Parameterization, calibration and evaluation. *Ecological Modelling*, 2019, 401, pp.1-19. 10.1016/j.ecolmodel.2019.03.005 . hal-02087426

**HAL Id: hal-02087426**

**<https://hal.science/hal-02087426>**

Submitted on 30 Jan 2020

**HAL** is a multi-disciplinary open access archive for the deposit and dissemination of scientific research documents, whether they are published or not. The documents may come from teaching and research institutions in France or abroad, or from public or private research centers.

L'archive ouverte pluridisciplinaire **HAL**, est destinée au dépôt et à la diffusion de documents scientifiques de niveau recherche, publiés ou non, émanant des établissements d'enseignement et de recherche français ou étrangers, des laboratoires publics ou privés.

1 **Implementation of an end-to-end model of the Gulf of Lions ecosystem (NW**  
2 **Mediterranean Sea). I. Parameterization, calibration and evaluation**

3  
4 Bănanu Daniela\*<sup>1</sup>, Frédéric Diaz\*<sup>1</sup>, Philippe Verley<sup>2</sup>, Rose Campbell<sup>3</sup>, Jonathan Navarro<sup>1</sup>, Christophe  
5 Yohia<sup>1</sup>, Ricardo Oliveros-Ramos<sup>4</sup>, Capucine Mellon-Duval<sup>5</sup>, Yunne-Jai Shin<sup>6</sup>

6  
7 <sup>1</sup>Aix Marseille Université, Université de Toulon, CNRS, IRD, MIO UM 110, Mediterranean Institute  
8 of Oceanography, Marseille, France.

9 <sup>2</sup>IRD, UMR 123 AMAP, TA40 PS2, Boulevard de la Lironde, 34398 Montpellier Cedex 5, France.

10 <sup>3</sup>Ecole d'Ingénieurs en Génie des Systèmes Industriels (EIGSI). 26, rue François de Vaux de Foletier,  
11 17041 La Rochelle cedex 1.

12 <sup>4</sup>Instituto del Mar del Perú (IMARPE), Gamarra y General Valle s/n Chucuito, Callao, Peru.

13 <sup>5</sup>UMR MARBEC (IFREMER, IRD, UM, CNRS), 34203 Sète cedex, France.

14 <sup>6</sup>IRD, UMR 248 MARBEC, Université de Montpellier, Bat. 24 – CC 093 Place Eugène Bataillon  
15 34095 Montpellier Cedex 5, France.

16  
17 \*Corresponding Authors: Tel: +33 (0)486 090 625 (D. Bănanu) : +33 (0)486 090 564 (F. Diaz)

18 Email addresses: daniela.Bănanu@univ-amu.fr (D. Bănanu), frederic.diaz@univ-amu.fr (F. Diaz),

19 --

20  
21 Key words: ecosystem modelling, food web, fisheries, OSMOSE, Eco3M

22  
23 *Note: This manuscript is linked to the manuscript: “**Implementation of an end-to-end model***  
24 *of the Gulf of Lions ecosystem (NW Mediterranean Sea). II. Investigating the effects of*  
25 *high trophic levels on nutrients and plankton dynamics and associated feedbacks through*  
26 *a two-ways coupling approach” by Diaz et al. (2019). *Ecological Modelling* 405, 51-69,*  
27 *<https://doi.org/10.1016/j.ecolmodel.2019.05.004>*

29 **ABSTRACT**

30 An end-to-end model named OSMOSE-GoL has been built for the Gulf of Lions, the main French  
31 Mediterranean fishing area. This spatialized dynamic model links the coupled hydrodynamic and  
32 biogeochemical model Eco3M-S/SYMPHONIE (LTL - low trophic level model) to OSMOSE  
33 (HTL - high trophic level model). It includes 15 compartments of living organisms, five from the  
34 LTL model (*i.e.* nanophytoplankton, microphytoplankton, nanozooplankton, microzooplankton and  
35 mesozooplankton) and ten from the HTL model (northern krill, southern shortfin squid, European  
36 pilchard, European anchovy, European sprat, Atlantic horse mackerel, Atlantic mackerel, blue  
37 whiting, European hake and Atlantic bluefin tuna). With the exception of northern krill and  
38 European sprat, all HTL species are commercially exploited and undergo fisheries mortality  
39 pressure. The modeled species represent more than 70% of annual catches in this area. This paper  
40 presents the parameterization, calibration and evaluation of this model with satellite data for  
41 phytoplankton and with biomass, landings, diet and trophic level data for HTL groups. For most  
42 species, the diets in output of OSMOSE-GoL are similar to field and literature data in terms of  
43 dominant prey groups and species. However, some differences were observed. Various reasons may  
44 explain the mismatch between the modelled diet and field data. Benthic prey sometimes observed in  
45 the stomach content of the HTL predators were not modelled in OSMOSE-GoL. Field studies were  
46 carried out at specific periods and locations, while our data concern the period 2001-2004 and the  
47 entire modelled domain. Inter- and intra-annual variations in spatial distribution and density of prey  
48 may also explain these differences. The model estimates trophic level values similar to those cited  
49 in the literature for all the HTL compartments. These values are also close to the trophic levels  
50 estimated by a previous Ecopath model for the same area and period. Even though some  
51 improvements are still possible, this model may already be of use to explore fishery or Marine  
52 Protected Areas scenarios for socio-ecosystem management issues.

53

## 54 **1. Introduction**

55 End-to-end (E2E) models are particularly appropriate to disentangle the intricacy of  
56 interactions occurring between physical forcing and low and high trophic level communities in the  
57 context of a quantitative approach dedicated to Ecosystem-Based Management (EBM) (*e.g.* Travers  
58 et al., 2007; Rose, 2012). They use multiple field data sets and are able to assess and simulate the  
59 dynamics of the main descriptors of the ecosystem rather than evaluating single resources and  
60 single threats (Shin et al., 2010; Christensen and Walters, 2011; Collie et al., 2016). Similar  
61 approaches, driven by modeling and information are used not just in ecology, but in many other  
62 areas to improve, and in some cases save our lives (Helbing et al., 2015).

63 However, the implementation of end-to-end modelling remains challenging, mainly due to the  
64 major differences between the sub-models of hydrodynamics and Low Trophic Level (LTL)  
65 organisms on the one hand, and that of High Trophic Level (HTL) organisms on the other hand (see  
66 review by Rose et al., 2010). The challenges are numerous and concern both concepts (*e.g.*  
67 representation of the zooplankton key level, differential scaling of processes, behavioral movement  
68 of HTL organisms, *etc.*) and technical issues (*e.g.* different programming languages and time-steps).  
69 One of the main challenges concerns the nature of link between sub-models. Travers et al. (2009)  
70 considered two possible types of links between LTL and HTL models. In the one-way forcing mode,  
71 LTL groups' biomasses serve as prey fields to HTL groups, without any feedback on the LTL  
72 compartments. In the two-ways coupling mode, the biomass of the LTL groups serve as prey field  
73 for HTL groups and an explicit rate of HTL-induced predation is specifically applied as feedback on  
74 each of the LTL groups.

75 Over the last decade, E2E modelling studies applied to regions or to the whole basin of the  
76 Mediterranean Sea have flourished in the context of EBM (Coll and Libralato, 2012). This research  
77 trend has been mainly driven by the more and more numerous observations of increasing threats  
78 and impacts on the Mediterranean marine ecosystems due to the exponential development of  
79 anthropogenic activities (*e.g.* Lötze et al., 2011; Coll et al., 2012). Most of these modelling studies

80 have been based on the Ecopath with Ecosim (EwE) model (see review of Coll and Libralato,  
81 2012), and only a few have used alternative models, spatial and multispecies models such as the  
82 OSMOSE size-based model (Halouani et al., 2016), or age-structured models applied to single  
83 species (*e.g.* Santojanni et al., 2005).

84 Furthermore, while implementation of the EBM of the Gulf of Lions (GoL) is particularly crucial  
85 owing to its major contribution to Mediterranean fisheries catches (Sánchez, 2008; Demaneche et al.,  
86 2009), this shelf area has been poorly investigated to date (Coll and Libralato, 2012). Only the  
87 recent study by Bănaru et al. (2013) dealt with the fishing impact on the trophic structure of the  
88 marine ecosystem using an EwE approach. However, this study is not spatialized and is based on  
89 some crude assumptions, concerning for example the plankton compartment (prey for the  
90 planktivorous fish species), for which the biomass level is determined from the literature and  
91 satellite imagery. A major bias of this type of modelling approach is that it does not account for the  
92 close coupling between the physical and biological (*sensu largo*) processes. Yet these interactions  
93 occur at multiple spatial and temporal scales in the NW Mediterranean Sea, and it has now been  
94 well-demonstrated that they have a significant impact on the dynamics and the spatial distribution  
95 of marine organisms from plankton to top predators (*e.g.* Fromentin et al., 2003; Niewiadomska et  
96 al., 2008; Cotté et al., 2011; Campbell et al., 2013). It is therefore necessary to represent the Gulf of  
97 Lions ecosystem more realistically, in particular the environmental forcing, the spatial dynamics of  
98 living organisms and their interactions, to enable a finer analysis of the functioning of the  
99 ecosystems and *in fine* to plan its optimal management for the next decades.

100 The E2E approach developed in this study is based on a fully dynamic coupling (*i.e.* two-ways  
101 coupling) of two pre-existing sub-models representing the dynamics of LTL organisms driven by  
102 hydrodynamics and climate processes on the one hand, and the dynamics of HTL organisms  
103 impacted by fishing activities on the other hand. The first model component is the Eco3M-  
104 S/Symphonie model that has been successfully used in the North-Western Mediterranean Sea to  
105 advance our understanding of the influence of hydrodynamics and atmospheric drivers on the

106 distribution of plankton at different spatial and temporal scales (*e.g.* Auger et al., 2011, 2014;  
107 Campbell et al., 2013; Clotti et al., 2014). The second component model is the individual- and  
108 size-based model OSMOSE (Shin and Cury, 2004). This HTL model has been applied worldwide in  
109 order to achieve better understanding of the functioning of diverse marine ecosystems (*e.g.* Travers et  
110 al., 2006; Mørzloff et al., 2009; Fu et al., 2013; Grüss et al., 2015, 2016; Houlihan et al., 2016).  
111 The aim of the present paper is to document an E2E model developed for the GoL (the OSMOSE-  
112 GoL model) and based on dynamic feedback (two-ways coupling) between two pre-existing LTL  
113 and HTL sub-models. Numerous data sets available in this marine region have been used to  
114 calibrate and quantitatively evaluate both the LTL and the HTL modules of the OSMOSE-GoL  
115 model. **An application of this model that consists in an analysis of the impacts of the predation  
116 pressure exerted by HTL planktivorous species on the spatial distributions, the structure of the LTL  
117 community and food webs controls is presented in a companion paper (Diaz et al., 2019).**

118

## 119 **2. Methods**

### 120 2.1. The E2E modelling approach

121 The approach developed in this study is based on the coupling of two existing sub-models.  
122 The first is the Eco3M-S/Symphonie model (Campbell et al., 2013) that represents the dynamics of  
123 Low Trophic Level (LTL) organisms driven by hydrodynamics and climate processes. The second is  
124 the individual-based model OSMOSE (Shin and Cury, 2004; Grüss et al., 2015), that simulates the  
125 dynamics of High Trophic Level (HTL) organisms. Both models have been fully described in  
126 previous works, therefore only the main characteristics are given hereafter. They are coupled in two  
127 distinct modes (Figure 1). In the one-way forcing mode, the biomass outputs of the LTL model are  
128 provided as inputs for the OSMOSE model without any feedback on the LTL biomass. In the two-  
129 ways coupling mode, there is a dynamic feedback between the two models through the predation  
130 process: the biomass outputs of the LTL model are provided as inputs for the OSMOSE model,  
131 which provides in return an additional rate of predation by the HTL planktivorous organisms.

132

### 133 2.1.1. Description of the LTL model

134 The LTL model is composed of two coupled models: the Symphonie hydrodynamic model  
135 and the Eco3M-S biogeochemical model (Campbell et al., 2013). The meteorological and  
136 hydrodynamic processes influencing the spatial and temporal distributions of nutrients and plankton  
137 were simulated by the Symphonie model (Marsaleix et al., 2008), a 3-D primitive equation, free  
138 surface model, based on hydrostatic and Boussinesq approximation. This model has already been  
139 used to successfully represent certain physical processes in the Northwestern Mediterranean Sea  
140 (*e.g.* Dufau-Julien et al., 2004; Ulses et al., 2008; Kersalé et al., 2013). The Symphonie version  
141 used here has been developed by Hu et al. (2011a). The modeled zone (711 km by 303 km) extends  
142 over the NW Mediterranean Sea, including the whole of the Gulf of Lions and parts of the Ligurian  
143 and Catalan Seas (Fig. 2). The grid used a square horizontal mesh with a spatial resolution of 3 km  
144 by 3 km. Sigma coordinates were used on the vertical dimension with a maximum of 40 levels. The  
145 model was run from January 9, 2001 to December 24, 2004. All details on the initial and boundary  
146 conditions are given in the studies of Hu et al. (2011a) and Campbell et al. (2013).

147 The biogeochemical model Eco3M-S is embedded in the Eco3M platform (Baklouti et al., 2006a,b),  
148 and is a multi-nutrient and Plankton Functional Types (PFT) model that simulates the dynamics of  
149 several biogeochemical decoupled cycles of biogenic elements (carbon, nitrogen, phosphorus and  
150 silica) and non-redfieldian plankton groups. The Eco3M-S version has been recently used and  
151 validated in the studies of Hu et al. (2011a,b) and Campbell et al. (2013) for the biogeochemical  
152 components and the hydrodynamics features, respectively. The model structure encompasses seven  
153 compartments of living organisms. Two of the three PFT of autotrophs of the model, from the  
154 smallest to the largest, were accounted for: (1) nano-phytoplankton, NANOPHY (2–20  $\mu\text{m}$ ) that  
155 dominate the biomass of phytoplankton assemblages for most of the year (Marty et al., 2002; Marty  
156 and Chiavérini, 2010), with a heterogeneous taxonomic composition (*e.g.* autotrophic dinobionts);  
157 and (2) the micro-phytoplankton community, MICROPHY (20-200  $\mu\text{m}$ ), largely dominated by

158 phytoplankton silicifiers (mainly diatoms) that can for certain periods contribute to a significant part  
159 of primary production and biomass during spring bloom in the NW Mediterranean Sea (Marty et al.,  
160 2002; Marty and Chiavérini, 2010). Three of the four PFTs of heterotrophs of the model, from the  
161 smallest to the largest, were considered: (1) nano-zooplankton, NANOZOO (5-20  $\mu\text{m}$ , mainly  
162 bacterivorous dinobionts and small ciliates) that consume the smallest phytoplankton groups ( $<2$   
163  $\mu\text{m}$ ) and bacteria; (2) micro-zooplankton, MICROZOO (20-200  $\mu\text{m}$ , mainly most of ciliates groups  
164 and large dinobionts), having characteristics (growth, ingestion rates) close to NANOZOO but with  
165 a wider prey spectrum, especially with potential consumption of micro-phytoplankton; and (3)  
166 meso-zooplankton, MESOZOO ( $>200$   $\mu\text{m}$ , mainly copepod groups but also including amphipods)  
167 grazing on the largest categories of plankton ( $>20$   $\mu\text{m}$ , micro-phytoplankton and micro-  
168 zooplankton) and producing fast-sinking fecal pellets. All the formulations of the biogeochemical  
169 processes, as well as the whole set of parameters, have been extensively described in Campbell et  
170 al. (2013). Constant mortality rates were applied to some of phytoplankton and zooplankton groups  
171 (Table 1), representing either senescence or viral attacks or predation.

172

### 173 2.1.2. Description of the HTL model

174 The OSMOSE (Object-oriented Simulator of Marine ecOSystEms, Shin and Cury, 2001;  
175 Shin and Cury, 2004) model (version Osmose 3.2, [www.osmose-model.org/downloads](http://www.osmose-model.org/downloads)) is a two-  
176 dimensional spatially explicit, individual-based model (IBM), written in Java ([www.osmose-  
177 model.org](http://www.osmose-<br/>177 model.org)), and based on the main assumption of opportunistic and size-based predation. OSMOSE  
178 is a multispecies model representing the whole life cycle of several interacting species, from eggs  
179 and larvae to juveniles and adults. At the first time step following the production of eggs, the total  
180 number of eggs of each population is split into super-individuals called “schools”, spatially  
181 distributed according to the input distribution maps.

182 At each time step, OSMOSE simulates the biological and ecological processes at the super-  
183 individual level: growth, predation and forage, reproduction, natural and starvation mortalities as

184 well as fishing mortality (Figure 1). The different sources of mortality of schools (fishing,  
185 predation, starvation and diverse mortality) occur in a random order. Two types of movements are  
186 considered in the OSMOSE-GoL model: (1) ontogenetic and seasonal migrations, taken into  
187 account through the use of distribution maps; and (2) small-scale random diffusion, when the  
188 distribution maps of schools (depending on fish age, stage, size, and season, year) does not change  
189 from one time step to the next.

190

### 191 2.1.3. Technical details on the two-ways coupling mode

192 The two-ways coupling between the OSMOSE-GoL and Eco3M-S/Symphonie models was  
193 performed through the predation process. Outputs of plankton groups provided by the LTL model  
194 serve as prey fields for the HTL organisms, which return an additional predation mortality in the  
195 plankton groups. To circumvent the different spatial dimensions (3D vs. 2D) and units (mmolN (or  
196 C)  $m^{-3}$  vs. tons wet weight) of the two models, plankton concentrations were vertically integrated  
197 and converted into biomass using conversion factors (Table 1). Only a small portion of plankton  
198 biomass is available to fish and macroinvertebrates due to various processes affecting their vertical  
199 distribution (turbulence, migrations, *etc.*). Availability of plankton to HTL species is not easy to  
200 assess in the field, and literature on this point is non-existent. Therefore, the availability parameters  
201  $a_p$  ( $p$  for a given plankton group  $p$ ) were estimated (Table 2) *via* the calibration of the model (see  
202 hereafter).

203 The two-ways coupling mode meant that the HTL model returns a specific mortality rate for each  
204 plankton group over space and time, and these rates were computed from the amount of prey  
205 ingested, as described in Travers et al. (2009). In each cell  $(x,y)$  of OSMOSE-GoL and for each  
206 plankton group ( $p$ ), the HTL-induced mortality rate at time  $t+\Delta t$  was computed as the total biomass  
207 of plankton eaten ( $BE_{\Delta t}$ ) during the time step  $\Delta t$  (15 days) over the mean total plankton biomass  
208 ( $B$ ) at time  $t$  multiplied by  $\Delta t$  (Eq. (1)). As the maximum biomass of plankton  $p$  eaten by HTL  
209 organisms at time  $t+\Delta t$  is the available biomass  $a_p \cdot B(x, y, t, p)$  at time  $t$ , the HTL-induced

210 mortality rate can thus vary between 0 and  $\frac{a_p}{\Delta t}$ . Because this variable mortality was added to the  
 211 natural mortality ( $m_p$ ) already considered in the Eco3M-S model (Table 1), the latter rate was  
 212 reduced to  $(m_p - \frac{a_p}{2 \cdot \Delta t})$ , with  $(\frac{a_p}{2 \cdot \Delta t})$  being the median of the variable mortality due to HTL  
 213 species. It was not set to zero in order to account for other sources of mortality such as predation by  
 214 non-modelled organisms, senescence and starvation mortality. Outside the common domain  
 215 between the Eco3M-S/Symphonie and OSMOSE-GoL models (Figure 2), the plankton mortality  
 216 rate was set to  $m_p$ .

$$217 \quad m(x, y, z, t + \Delta t, p) = \frac{BE_{\Delta t}(x, y, p)}{\Delta t \cdot B(x, y, t, p)} + \left( m_p - \frac{a_p}{2 \cdot \Delta t} \right) \quad (1)$$

218 According to the equation (1), the plankton total mortality rate thus ranges between  $m_p - \frac{a_p}{2 \cdot \Delta t}$  and  
 219  $m_p + \frac{a_p}{2 \cdot \Delta t}$ . This rate can be either lower or higher than the initial mortality rate  $m_p$  depending on  
 220 the predation pressure induced by HTL organisms.

221

#### 222 2.1.4. Design of the numerical experiment

223 A first spin-up period of 35 years was launched in the one-way forcing mode to reach  
 224 equilibrium of the HTL model outputs. This step was achieved using the numerical fields of  
 225 plankton biomass in 2001. Following this period of spin-up, the model was then run in the one-way  
 226 forcing mode (years 36 and 39) using the plankton biomass in 2001, and then in the two-ways  
 227 coupling mode for four years (40 to 43). For the last four years (40 to 43), the HTL model received  
 228 the numerical fields of LTL biomass for the years 2001 to 2004. These years was chosen because  
 229 the LTL model has been previously validated over this period (Campbell et al., 2013). The coupling  
 230 simulation started on January 10, 2001 (00h00) and it ended on December 20, 2004 (00h00). Years  
 231 36 to 39 (one-way forcing) as well as the period of two-ways coupling mode (years 40 to 43) were

232 considered for analysis hereafter. Furthermore, a set of 50 replicated simulations was run to account  
233 for the stochasticity of the OSMOSE model.

234

## 235 2.2. Parameterization of the HTL model

### 236 2.2.1. Modelled domain and selected HTL groups

237 In this study, the OSMOSE-GoL model grid consists of 19 by 15 cells with a resolution of  
238 12 km by 12 km covering the GoL area north of a line running from 42°04' -3°18' to 43°05' -5°37'  
239 (Figure 2). A set of 25 schools released per time step per species (600 per year per species) was  
240 chosen for this model as a compromise between the stochasticity of the model and numerical  
241 limitations in memory and calculation speed.

242 As simulations with OSMOSE necessitate extensive information on entire life cycles, only 10 HTL  
243 key species, being the most representative of the pelagic and demersal food web, were included in  
244 the configuration of OSMOSE GoL: northern krill (*Meganyctiphanes norvegica*, (Sars 1857)),  
245 southern shortfin squid (*Illex coindetii*, (Vérany 1837)), and eight fish species from small pelagic  
246 fish to demersal fish: European pilchard (*Sardina pilchardus*, (Walbaum 1792)), European anchovy  
247 (*Engraulis encrasicolus*, (Linnaeus 1758)), European sprat (*Sprattus sprattus*, (Linnaeus 1758)),  
248 Atlantic horse mackerel (*Trachurus trachurus*, (Linnaeus 1758)), Atlantic mackerel (*Scomber*  
249 *scombrus*, (Linnaeus 1758)), blue whiting (*Micromesistius poutassou*, (Risso 1827)), European hake  
250 (*Merluccius merluccius*, (Linnaeus 1758)), Atlantic bluefin tuna (*Thunnus thynnus*, (Linnaeus  
251 1758)). These species represent more than 70% of annual catches (Demaneche *et al.*, 2009). Some  
252 of them were selected because of their importance for fisheries (European pilchard, European  
253 anchovy, Atlantic horse mackerel, Atlantic mackerel, European hake, Atlantic bluefin tuna) (SIH,  
254 2017), others for their importance as forage species such as northern krill, European sprat and blue  
255 whiting (Bănaru *et al.*, 2013). All these species represent the most important ones in terms of  
256 structure and functioning of the food web in this area (Bănaru *et al.*, 2013).

257 To parameterize the model, various input information items were needed, including: (1) spatial  
258 distribution maps for different life stages and time steps (Appendix 1). These maps coded for  
259 presence *vs.* absence for each species. They have been obtained from geo-referenced data of the  
260 PELMED and MEDITS research surveys conducted since 1993 (IFREMER databases). Atlantic  
261 bluefin tuna is the sole highly migratory species with only a seasonal presence in the modelled area  
262 and not reproducing in the GoL (Imbert et al., 2007); (2) predation, growth and reproduction  
263 parameters (Table 4); (3) mortality parameters (Table 1); (4) fishing and reproduction seasonality  
264 (see sections 2.2.2 and 2.2.3).

265

#### 266 2.2.2. Predation, growth and reproduction processes

267 In the OSMOSE model, predation is assumed to be an opportunistic process and occurs  
268 when there is both size adequacy and spatio-temporal co-occurrence between predator and prey.  
269 Within a cell of the grid, a predator can feed on a co-occurring prey if: (1) the prey is of a suitable  
270 size, that is, within a range determined by the minimum and maximum predator/prey size ratios;  
271 and (2) the vertical distribution of the prey makes it accessible to the predator, which is determined  
272 by the accessibility coefficients provided to OSMOSE-GoL. Therefore, the food web (or diet  
273 matrix) builds up as an emergent property of local trophic interactions (Travers et al., 2009).  
274 Minimum and maximum predator/prey size ratios (Table 3) were parameterized differently for  
275 different size classes for each taxon, in order to account for ontogenetic changes in feeding  
276 behavior. These size ratios were built from local data on diet, predators and prey size (Labat and  
277 Cuzin-Roudy, 1996; Båmstedt and Kørnø, 1998; Imbert et al., 2007; Le Luherne, 2012;  
278 Bourgogne, 2013; Le Bourg et al., 2015; Mellon-Duval et al., 2017).  
279 The accessibility coefficients were set by default at 0.8 for HTL groups. For some species, these  
280 coefficients were reduced to 0.6 in relation to their exclusive benthic location during early life  
281 stages (northern krill <1 cm, southern shortfin squid <2 cm and European hake <6 cm), or to the  
282 very coastal area distribution patterns of individuals <5 cm and thus low accessibility to predation

283 (0.6 for European pilchard and anchovy and 0.4 for European sprat) (Labat and Cuzin-Roudy, 1996;  
284 Mellon-Duval et al., 2017; Bănar, pers. comm.; Bigot, pers. comm.).

285 During the predation process, if enough prey items are present in a spatial cell, a predator feeds  
286 upon them uniformly until it reaches satiation. Predation efficiency is defined as the ingested prey  
287 biomass over the maximum biomass a predator can feed upon. For each species, the maximum  
288 ingestion rates (MIR, Table 3) have been assessed from local data (Palomares and Pauly, 1998;  
289 Bănar et al., 2013). However, some of the considered species consume a non-negligible part of  
290 benthic prey that was not considered in the Osmose-GoL model. In order to avoid artificially  
291 increasing predation on pelagic and demersal prey, their MIR were proportionally reduced by 35%  
292 for southern shortfin squid, Atlantic horse mackerel, Atlantic mackerel and European hake (Kaci,  
293 2012; Le Luherne, 2012; Mellon-Duval et al., 2017) and by 12.5% for blue whiting (Bourgogne,  
294 2013). When the predator does not ingest enough food to fulfill its maintenance requirements  
295 (corresponding to a predation efficiency threshold of 0.57; Shin and Cury 2004), fish starve at a rate  
296 which decreases linearly with predation efficiency (Shin and Cury, 2004). The maximum mortality  
297 rate by starvation was fixed at  $1.0 \text{ year}^{-1}$ , applied during a time step in the absence of food.

298 Predation efficiency also determines fish growth rate during a time step. When the biomass of prey  
299 eaten is higher than maintenance requirements, the growth rate of fish is positive, varying as a  
300 function of the von Bertalanffy growth rate and the predation efficiency (Shin and Cury, 2004).

301 The growth parameters (Table 4) were computed from local studies (Farrugio et al., 1991;  
302 Campillo, 1992; SCRS, 1997; Mellon-Duval et al., 2009; GFCM-FAO, 2011a, b; PELMED and  
303 MEDITS, IFREMER campaigns). Longevity was estimated from literature data (Campillo, 1992;  
304 Labat and Cuzin-Roudy, 1996; Sánchez et al., 1998).

305 Predation success has also an indirect effect on the reproduction process through the biomass of  
306 spawners which, combined with relative fecundity parameters, defines the number of eggs released  
307 in the system. Any school of the key populations, whose size is greater than the sexual maturity size  
308 ( $S_{\text{mat}}$ ), reproduces according to the spawning seasonality and to the species relative annual fecundity

309 ( $\phi$ , number of eggs spawned per gram of mature female per year) (Shin and Cury, 2004).  
310 Data for size at maturity ( $S_{mat}$ ) are indicated in Table 4 (Higginbottom and Hosie, 1989; Farrugio et  
311 al., 1991; Campillo, 1992; Labelle et al., 1997; Sánchez et al., 1998; Leonart, 2001; Sinovčić et al.,  
312 2004; GFCM-FAO, 2011; www.fishbase.org; PELMED and MEDITS, IFREMER campaigns).  
313 Sex ratio was hypothetically fixed at 0.5.  
314 The relative fecundity (Table 4) has been recomputed considering the number of eggs using data  
315 from Ross and Quentin (1986), Campillo (1992), Laptikhovsky and Nigmatullin (1993), Quero and  
316 Vayne (1997), Sánchez et al. (1998), and the estimated weight of mature females based on the total  
317 length for each species.  
318 Seasonality of reproduction was estimated using data from Farrugio et al. (1991), Campillo (1992),  
319 Labat and Cuzin-Roudy (1996), PELMED and MEDITS, IFREMER campaigns. Egg weight (0.54  
320 mg) and size (S) (Table 4) were also indicated in the model (Quero and Vayne, 1997; Le Bourg,  
321 pers. comm.) as eggs represent potential prey for the rest of the food web.

322

### 323 2.2.3. Fishing and natural mortality processes

324 Fishing pressure is represented through a population-specific fishing mortality rate  $F$  (Table  
325 2), affecting the number of fish per school when larger than the specified size of recruitment to  
326 fisheries. Legal size of catch ( $S_{rec}$ , Table 4) has been used as recruitment size in the OSMOSE-GoL  
327 model. Initial estimates of annual fishing mortality rates have been estimated for each target  
328 species, using the landings to biomass ratio obtained from stock assessments (PELMED, MEDITS,  
329 GCFM) and from the fisheries database (SIH, 2017). These mortality rates were subsequently  
330 refined through the calibration of the model (see 2.3). Fishing mortalities are assumed to be  
331 spatially homogeneous, but can vary seasonally as specified in input (Table 5). Fishing seasonality  
332 was estimated using catch data by species (SIH, 2017).

333 In addition to explicit predation mortality modelled in Osmose, the mortality of the first life stages  
334 (eggs and first feeding larvae,  $M_0$ , Table 2) is due to different natural causes (*e.g.* non-fertilisation of

335 eggs, starvation of first feeding larvae, advection, sinking) as well as predation by organisms not  
336 considered in the OSMOSE-GoL model. Additional sources of natural mortality concerning other  
337 life stages have also been accounted for ( $M_s$ , Table 2), including mortality due to disease,  
338 senescence and predation by organisms not represented in the OSMOSE-GoL model (*e.g.* birds,  
339 mammals, *etc.*). Since it is usually very hard to quantify these types of mortality, they have been  
340 assessed through the calibration of the model for each of the ten HTL species.

341

### 342 2.3. Calibration for the HTL model

343 The OSMOSE-GoL model has been calibrated using an optimization technique based on an  
344 evolutionary algorithm, and a maximum likelihood based objective function, so that the modeled  
345 biomass and landings of the ten HTL species remained within realistic observed ranges. The data  
346 sources used for the biomass are from the PELMED and MEDITS cruises performed every year in  
347 June and July from 2000 to 2013 and GFCM-FAO stock assessments for the GoL (Jadaud, pers.  
348 comm.; Bigot, pers. comm.; Sfrux, pers. comm.), VPA models for hake and tuna (Jadaud, pers.  
349 comm.; Fromentin, pers. comm.) and SIH (2017) for landings.

350 The calibration was performed with the `calibraR` package (Oliveros-Ramos et al., 2015; Oliveros-  
351 Ramos and Shin, 2016; <https://CRAN.R-project.org/package=calibrar>) that has been specifically  
352 developed for calibrating complex ecological models, and `osmose2R` ([http://www.osmose-](http://www.osmose-model.org)  
353 [model.org, https://CRAN.R-project.org/package=osmose](https://CRAN.R-project.org/package=osmose)), which includes a set of R functions for  
354 interfacing Osmose with `calibraR`.

355 The calibration step aimed at providing estimates of the following parameters of the model: (i)  
356 availability coefficients of plankton groups to HTL species, (ii) larval mortality rate for each species  
357 and (iii) fishing mortality rates for each species (Table 3). These parameters have been selected  
358 because they are highly model-dependent, *i.e.* their meaning depends on the model structure and  
359 assumptions, and there are no reasonable initial estimates for plankton accessibility and larval  
360 mortality (Oliveros-Ramos et al., 2015). The objective function minimized by the algorithm is built

361 automatically by the R package by aggregating lognormal-likelihood functions that quantify the fit  
362 between model outputs and field observations. Biomass and landings from year 2001 were given to  
363 the algorithm for every modeled species as the observed data, and the OSMOSE-GoL model was  
364 forced with the LTL biomass of the Eco3M-S/Symphonie model from the same year. In this way, a  
365 “steady-state” calibration of the OSMOSE-GoL model has been achieved for year 2001, that is the  
366 first year of the coupled simulation.

367 The calibration step enabled us to obtain a set of parameters so that biomass and landings of the  
368 considered HTL species best range between the minima and maxima of the observed biomass in the  
369 GoL. This parameter set was then used in the coupled model.

370

## 371 2.4. Datasets for the evaluation of the E2E model

### 372 2.4.1. Evaluating phytoplankton biomass of the LTL model using remote sensing satellite data

373 Ocean color data from the GlobColour project ([www.glocolour.info/](http://www.glocolour.info/)) were used in this study  
374 to evaluate the realism of the modelled surface chlorophyll *a* concentrations (considered as a proxy  
375 of phytoplankton biomass). The GlobColour product takes advantage of gathering data sets derived  
376 from several ocean color sensors (ENVISAT, MODIS, MERIS and SeaWiFs). Three sensors  
377 (SeaWiFS, MERIS and MODIS) showed a temporal overlap of functioning from April 2002 to  
378 December 2010, and it was possible to perform a quantitative comparison between satellite and  
379 modeled chlorophyll *a* values over most (990 days) of the modelled period (1440 days).

380 The GlobColour product provided a weighted mean ( $\overline{Chl_w}$ ) and a weighted error ( $\varepsilon(\overline{Chl_w})$ ). The  
381 detailed computation of these parameters is given in the Product User Guide of GlobColour  
382 available on the aforementioned web site.

383 In order to accurately compare the concentrations of the satellite-derived chlorophyll *a* to those  
384 modeled, the numerical concentrations of total chlorophyll (sum of chlorophyll *a* concentrations of  
385 pico-, nano- and microphytoplankton) were averaged over the first optical layer (*sensu* Bricaud et  
386 al., 2010),  $\overline{Chl_{opt1}}$ . The details of the computation are given in the recent study of Campbell et al.

387 (2013). The model-derived chlorophyll *a* values were re-interpolated point by point at the size of  
 388 each pixel (1.1 km) of the satellite image on the modeled domain. The period of assessment (990  
 389 days) was characterized by more than a third (~34%) of cloudy days without useable pixels on the  
 390 modeled area, therefore the comparison was made on the remaining days, corresponding to a total  
 391 of 236877 pixels.

392 A metric of model to data comparison (C parameter) was built and used hereafter. This metric  
 393 assessed the size of the discrepancies between the predicted and satellite values as follows:

$$394 \quad C = \begin{cases} 0, & \text{if } \overline{Chl_{opt1}} \in [\overline{Chl_w} - \varepsilon(\overline{Chl_w}), \overline{Chl_w} + \varepsilon(\overline{Chl_w})] \\ \min \left\{ \left| \overline{Chl_{opt1}} - (\overline{Chl_w} + \varepsilon(\overline{Chl_w})) \right|, \left| \overline{Chl_{opt1}} - (\overline{Chl_w} - \varepsilon(\overline{Chl_w})) \right| \right\}, & \text{otherwise} \end{cases}$$

395

#### 396 2.4.2. Evaluating the HTL model using diet and trophic level data

397 Diet data for each of the modeled HTL species obtained as output of the OSMOSE-Gol  
 398 model were compared with *in situ* field data obtained from stomach content analyses (Le Bourg et  
 399 al., 2015; Bănaru, 2015; Bănaru, pers. comm.) or literature data (Båmstedt and Kjørson, 1998; Sara  
 400 and Sara, 2007; Mellon-Duval et al., 2017) for similar individual sizes.

401 Estimated trophic levels (TL) from the OSMOSE-Gol model were compared with TL values from  
 402 the literature based on the stomach content (Båmstedt and Kjørson, 1998; Stergiou and Karpouzi,  
 403 2002; Bănaru, 2015; Bănaru et Harmelin-Vivien, 2017) and compared with those of a local  
 404 ECOPATH model (Bănaru et al., 2013).

405 The aim of these comparisons was to check whether the parameterization and the processes of the  
 406 model were able to reproduce trophic interactions close to those observed in field data.

407

### 408 3. Results and discussion

#### 409 3.1. Calibrated biomass and landings of the HTL model against data

410 The calibration of the model enabled us to estimate some parameters of the HTL model such

411 as the accessibility coefficients of the plankton and larval mortality of HTL species, and to refine the  
412 fishing mortality estimates. The success of this calibration step lies in the ability of the model, once  
413 run with this set of calibrated parameters, to provide results remaining within realistic ranges for the  
414 biomass and landings of HTL species. The modeled median biomass (Figure 3) and landings (Figure  
415 4) of the ten HTL species and their corresponding envelopes delimiting 0.25 and 0.75 percentiles are  
416 presented for years 36 to 39 in the one-way forcing configuration. The modeled biomass and landings  
417 for years 40 to 43, resulting from the two-ways coupling mode, are presented and discussed in the  
418 companion paper (Diaz et al., 2019) for the detailed comparison with one-way forcing mode effects.  
419 Most of the modeled biomass of HTL species showed seasonal patterns of change in median values  
420 within the ranges of the field observations (Figure 3), except for that of European hake, which is  
421 slightly overestimated. The biomass of certain species such as the European hake is known to be  
422 underestimated, due mainly to the difficulty of catching large individuals during scientific surveys  
423 (Bigot, pers. comm.). The median simulated biomass of northern krill (Figure 3A) showed a seasonal  
424 dynamic with the highest values occurring in winter and the lowest at the end of the spring. The  
425 seasonal patterns of change of southern shortfin squid (Figure 3B) showed median levels of biomass  
426 around  $2.5 \times 10^4$  tons, with maximum values at the end of summer and minimum values at the end of  
427 winter. The stock of European pilchard (Figure 3C) showed cyclical variations around  $2 \times 10^5$  tons,  
428 with maxima reached in spring and minima at the beginning of the winter. The median biomass of  
429 European anchovy (Figure 3D) showed cyclical seasonal variations centered on  $10^6$  tons, and  
430 characterized by highest biomass from mid-winter to the end of spring, and the lowest during autumn.  
431 The seasonal variation of the European sprat (Figure 3E) biomass was very low. The median levels  
432 were around  $1 \times 10^4$  tons, with a barely discernible peak at the end of summer. The seasonal dynamics  
433 of Atlantic horse mackerel (Figure 3F) showed an increase in biomass at the end of autumn. A very  
434 weak seasonal signal in the biomass of Atlantic mackerel was simulated (Figure 3G), with the highest  
435 biomass extending from winter to mid-spring, and a minimum occurring from mid-summer to mid-  
436 autumn. The biomass of blue whiting (Figure 3H) did not show any clear seasonal pattern and

437 oscillated around  $4 \times 10^4$  tons. The temporal changes of European hake biomass (Figure 3I) also  
438 showed a very weak seasonal signal, with values around  $1.4 \times 10^4$  tons. By contrast, the biomass of  
439 Atlantic bluefin tuna (Figure 3J) showed a marked seasonal cycle, with a minimum of biomass during  
440 winter ( $\sim 5 \times 10^3$  -  $5.5 \times 10^3$  tons), followed by a sharp increase to reach a first seasonal maximum at  
441 the beginning of the spring ( $\sim 5.6 \times 10^3$  -  $6.2 \times 10^3$  tons). Another biomass minimum occurred at the  
442 beginning of summer, and then the annual peak (around  $7 \times 10^3$  tons) is observed in autumn. There  
443 were no seasonal biomass field data to use for comparison with model output, as scientific surveys  
444 were only organized during summer.

445 On the whole, for most of the HTL species, the whole or at least *pro parte* interannual dynamics of  
446 modeled median landings (and the corresponding range of percentiles) were within the ranges of  
447 observed data (Figure 4). However the median landings of southern shortfin squid (Figure 4B) and  
448 of Atlantic mackerel (Figure 4F) were much higher than those observed, by a factor of 16 ( $\sim 800$  tons)  
449 and 2.5 ( $\sim 500$  tons) with regard to observed landings, respectively, without any marked seasonal  
450 pattern. A possible explanation for this discrepancy could be the underestimation of the landings of  
451 southern shortfin squid and Atlantic mackerel in SIH (2017) landings databases, as for many other  
452 demersal and benthic species, because fishermen often directly sell their fish at local markets  
453 (CRPMEM PACA, 2016). Landings of northern krill and European sprat (Figures 4A and 4E) are not  
454 computed by the model as they are not landed by fishermen. The simulated temporal dynamics of  
455 planktivorous fish such as European pilchard and European anchovy showed marked and steady  
456 seasonal cycles. The median landings for European pilchard (Figure 4C) were minimum ( $\sim 180$  tons)  
457 at the beginning of winter. They rapidly increased during winter and reached a relative maximum  
458 ( $\sim 400$  tons) at the beginning of spring. Then, they briefly fell below 400 tons and again increased up  
459 to their absolute maximum ( $\sim 750$  tons) at the beginning of summer. They sharply decreased from the  
460 middle of summer to the end of the autumn down the absolute minimum. Maximum simulated values  
461 were higher than the maximum observed values during the first half of summer. The simulated  
462 landings of European anchovy (Figure 4D) also showed a minimum ( $\sim 100$  tons) at the beginning of

463 winter, but the catch then increased very rapidly up to a first peak of ~180 tons, and an absolute  
464 maximum (~250 tons) at the end of spring. The summer season is marked by a sharp decrease in  
465 landings, and a third peak of landings (~200-220 tons) in autumn. The whole set of seasonal modeled  
466 values remained within the range of observed landings. The seasonal changes in median landings for  
467 Atlantic horse mackerel (Figure 4F) were characterized by two maxima in spring and autumn. The  
468 spring maximum comprised between 20 and 28 tons was generally higher than the autumn maximum  
469 (<20 tons). In parallel, minima (around 10 tons or lower) were simulated during winter and summer.  
470 Only the maximum values of landings during spring and autumn fell within the range of observed  
471 landings. The temporal patterns of change in simulated landings for blue whiting (Figure 4H) showed  
472 a very marked seasonal trend. Median landings were close to zero from the beginning of summer to  
473 the end of autumn, they sharply increased to reach ~40 tons at the beginning of spring, and then  
474 drastically dropped during spring. The modeled landings were underestimated during the first half of  
475 the year. The median landings of the European hake (Figure 4I) remained around 100 tons from mid-  
476 winter to the end of summer within the range of observed landings during this period of year. They  
477 fell sharply during autumn to well below the lower limit of observed data, with a minimum of ~10  
478 tons, before increasing again at the beginning of winter. Modeled landings of Atlantic bluefin tuna  
479 (Figure 4J) were close to zero only over a short period of the year, mainly from the end of autumn to  
480 the beginning of winter. Catches sharply increased up to 250 tons during spring, before slightly  
481 declining to just below 200 tons at the beginning of summer. Summer was marked by an abrupt  
482 increase in the catches, reaching 500 tons at the end of summer. This seasonal cycle is characterized  
483 by simulated landings that were close to field data.

484

### 485 3.2. Comparing phytoplankton surface biomass of the LTL model with ocean color data

486 The seasonal cycle of surface satellite-derived chlorophyll *a* content averaged over the  
487 modeled area from April 2002 to December 2004 (Figure 5) is typical of those usually observed at  
488 oceanic mid-latitudes (*e.g.* Siegel *et al.*, 2002), with average minima during summer months and

489 maxima from winter to late spring. The very low summer concentrations ( $\sim 10^{-1}$  mg m<sup>-3</sup> or lower)  
490 are considered as representative of the Mediterranean Sea (Bosc et al., 2004). As expected, the  
491 seasonal pattern found during the study period was close to the “bloom” trophic regime according  
492 to the classification of D’Ortenzio and Ribera d’Alcalà (2009) for the Mediterranean Sea.  
493 An interannual variability of the seasonal cycle could be detected, with the year 2003 being  
494 characterized by a longer summer period of low chlorophyll *a* than 2002 and 2004. The year 2003  
495 did not show any clear autumnal bloom, while it was particularly marked in mid-September 2002  
496 and September and November 2004. The inter-annual variability in the phytoplankton surface  
497 content in this area of the Mediterranean Sea is a common feature that has been already observed in  
498 some other remote sensing time-series (Bosc et al., 2004; Auger et al., 2014) and in situ data (*e.g.*  
499 Marty and Chiavérini, 2010; Gernez et al., 2011).

500 Beyond the seasonal dynamics, the time-series highlights the variability of mean values at very high  
501 frequency (*i.e.* day-to-day), whatever the season considered. Most of the time, large error bars also  
502 suggest a strong spatial heterogeneity of phytoplankton content in the NW Mediterranean Sea. This  
503 variability at high frequency and the strong spatial heterogeneity are mainly due to the multiple  
504 physical forcing occurring in this marine area, such as changing wind gusts that drive intricate  
505 (sub)-mesoscale hydrodynamic processes (*e.g.* eddies, see Hu et al., 2011a,b) and upwellings  
506 (Millot, 1999), river inputs discharging large amounts of nutrients throughout the year (*e.g.* Minas  
507 and Minas, 1989) and the large-scale circulation of the Northern Current sometimes intruding on  
508 the shelf (Petrenko, 2003). All the aforementioned physical processes interact together at different  
509 spatial and temporal scales, and play a key role in setting ocean dynamics, heat transport and  
510 biogeochemical budgets through intense upwelling of nutrients, subduction of plankton and  
511 horizontal stirring (see review of Lévy, 2008).

512 The LTL model was able to reproduce the seasonal signal and the inter-annual variability of  
513 phytoplankton surface concentrations. The model also captured the daily variability. However, the  
514 modeled concentrations were, most of the time, underestimated compared to the satellite-derived

515 means concentrations, especially during late spring and summer. It is crucial to keep in mind that  
516 ocean color data in the Mediterranean Sea have to be considered with caution, because the  
517 algorithms used to derive the chlorophyll *a* concentrations perform poorly in this regional sea  
518 (Gregg and Casey, 2004; Volpe et al., 2007 and references therein). These low performances are  
519 generally attributed to the particular composition (*i.e.* inorganic and organic matter) of the water  
520 column causing an overestimation of chlorophyll *a* surface concentrations for low values especially  
521 of chlorophyll (*i.e.* during summer and in oligotrophic waters). This bias between *in situ* data and  
522 values derived from algorithms would be furthermore accentuated in the area of the Rhone  
523 freshwater influence according to the study of Ouillon and Petrenko, (2005). The C parameter,  
524 assessing error between model output and data (see section 2.4.2.), was null during *ca.* 23% of the  
525 comparison period. This result means that the modeled chlorophyll value remained within the range  
526 of the error bars given by the GlobColour algorithm during a quarter of the simulation period.  
527 Furthermore, figure 6 shows the temporal changes in the GlobColour errors on chlorophyll *a*  
528 concentrations and of the C parameter. The GlobColour errors and the C parameter were the lowest  
529 ( $<1.25 \times 10^{-1} \text{ mg m}^{-3}$ ) during summer, especially in 2003 and 2004, when they were the most  
530 variable and highest from autumn to mid-spring. The C parameter was lower than the satellite  
531 sensor errors during *ca.* 71% of the comparison period, which is a rather satisfactory result.

532

### 533 3.3. Comparing modeled and observed diet of the HTL species

534 Figure 7 shows the modelled diet of every size class of the ten HTL species. In order to describe the  
535 diets emerging from the OSMOSE-GoL model, prey groups were classified into three categories  
536 according to their proportion (in biomass) in the predator's diet: main prey (>50%), secondary prey  
537 (from 10 to 50%), accessory prey (from 1 to 10%).

538 According to the model, the main prey of the Northern krill is microphytoplankton (~56%), while  
539 the secondary prey is microzooplankton (~35%). Mesozooplankton remains an accessory prey  
540 (~8%). This modelled diet, composed of phyto- and zooplankton in almost equal parts, is consistent

541 with the observations of Båmstedt and Karlson (1998) on krill of the Northeast Atlantic. According  
542 to this field study, northern krill may not survive on a diet only based on phytoplankton and needs  
543 to consume at least 40% of zooplankton.

544 The modelled southern shortfin squid mainly feeds on small teleosts (~77%) such as planktivorous  
545 European pilchard (~36%) and European anchovy (~21%), but also on juveniles of Atlantic horse  
546 mackerel (~9%) and blue whiting (~8%). Small squid (*i.e.* cannibalism) (~11%) are secondary prey,  
547 while northern krill (~8%) and mesozooplankton (~4%) are accessory prey of southern shortfin  
548 squid. This modelled diet is consistent with some *in situ* datasets (Bănar, 2015) showing a diet  
549 mainly composed by ~80% of teleosts. In the latter field study, southern shortfin squid prey on  
550 certain other groups, such as benthic decapods, but these groups were not represented in the  
551 OSMOSE-GoL model.

552 According to the model outputs, European pilchard larvae (<3 cm) mainly feed on  
553 mesozooplankton (~81%). This trophic behaviour for larvae are close to the results of Borme et al.  
554 (2009) in the Mediterranean Sea, showing a diet almost exclusively (~99%) composed of copepods  
555 in the size range of mesozooplankton. Larger individuals significantly change their diet, feeding on  
556 smaller prey, with microzooplankton (~51% of the diet of juveniles ranging between 3 and 12.5 cm,  
557 and ~52% for adults >12.5 cm) as main prey, and microphytoplankton as secondary prey (~44% of  
558 the diet of juveniles and ~43% for adults). The latter results are not in line with some recent dietary  
559 field studies based on the analysis of stomach content in the Gulf of Lions. According to the study  
560 of Le Bourg et al. (2015), juveniles of European pilchard as well as adults may prey quasi-  
561 exhaustively on mesozooplankton (~98% and 100%, respectively). However this mismatch between  
562 model outputs and observations has to be moderated, because the study of Bode et al. (2004)  
563 showed that the size of the prey generally decreases with increasing body length of European  
564 pilchard. Hence, adults may consume a larger part of phytoplankton according to the latter study. As  
565 phytoplankton prey are actually more easily digested, they are therefore more difficult to identify in  
566 stomach contents, which may explain the differences between the model and observations for this

567 fish species. Moreover, the study of Pethybridge et al. (2014) using analysis of fatty acids in adults  
568 of European pilchard confirms the assumption that its diet is mainly based on microplankton.  
569 The modelled European anchovy, including its larvae stage, has a diet similar to those of the  
570 juveniles and adults of European pilchard. All stages mainly feed on microzooplankton (~55% of  
571 the diet for larvae <3 cm, ~49% for juveniles ranging between 3 and 12.5 cm and ~44% for  
572 adults >12.5 cm). Their secondary prey is the microphytoplankton group (~39% for larvae, ~40%  
573 for juveniles and ~36% for adults). Mesozooplankton is only an accessory prey, representing about  
574 5% of the diet for larvae and juveniles, and around 7% for adults. The simulated diet of the larvae is  
575 close to observed data. Analyzing fatty acids content, Rossi et al. (2006) showed that  
576 microzooplankton and microphytoplankton are the prey most consumed by anchovy larvae.  
577 However, the modelled diet for adult anchovy is rather different from those resulting from the  
578 analysis of stomach content (Borme et al., 2009; Le Bourg et al., 2015). In the observations, as for  
579 the European pilchard, the proportions of microzooplankton and microphytoplankton may be  
580 underestimated due to a rapid digestion of these types of prey.

581 The modelled diet of European sprat juveniles is similar to those of juveniles and adults of the  
582 European pilchard and of all size classes of the European anchovy. The diet of the juveniles is  
583 composed of microzooplankton (~48% of the diet) and microphytoplankton (~34%). The proportion  
584 of consumed mesozooplankton (~14%) is higher than in the diet of the juveniles of the European  
585 sardine and anchovy, but is much lower than that observed in their stomach content (~100%),  
586 according to the study of Le Bourg et al. (2015). The modelled diet of European sprat larvae (<3  
587 cm) is mainly composed of mesozooplankton (~81%), which is consistent with previous  
588 observations (Dickmann, 2005). Mesozooplankton is furthermore the main prey for adults but in  
589 much higher proportions (~68%) than for the adults of European pilchard and anchovy (~4.5% and  
590 ~7%, respectively). Adults also consume, as secondary prey, some European pilchard larvae  
591 (~16%). In the model, the European sprat (including larvae and adults) thus appears to be more  
592 carnivorous than the European sardine and anchovy. This modelled output is in line with the dataset

593 of Pethybridge et al. (2014) based on the comparative analysis of the fatty acids content of these  
594 three pelagic species. In the model, pilchard eggs and larvae are another significant prey (~16%) for  
595 the adults of European sprat, as also observed in their stomach content (Le Bourg et al., 2015).  
596 The diet of the juveniles of Atlantic horse mackerel predicted by the model is composed of a  
597 dominant proportion of mesozooplankton (~62%) and a lesser proportion of fish larvae (~25%),  
598 while the study of Le Luherne (2012) based on the analysis of stomach content showed a dominant  
599 consumption of northern krill (~71% in proportion) and a lesser proportion (~21%) of benthic  
600 decapods (not modelled). These differences may result from opportunistic predation behaviour  
601 (making the diets highly variable between the sampling stations inside the GoL domain), as well as  
602 from some differences between the spatial domain of the model (entire GoL) and the specific  
603 locations of the sampling stations used in the study of Le Luherne (2012). Adults of Atlantic horse  
604 mackerel (>16 cm) have a modelled diet which is quite different from that of juveniles. They mainly  
605 feed on southern shortfin squid (~37%) and northern krill (~28%). Some other prey such as  
606 juveniles of European sprat and hake and Atlantic mackerel supplement their diet (~17%). The  
607 cumulated percentage of consumed fish is rather high (34%). The modelled proportion of northern  
608 krill consumed is close to that resulting from the analysis of *in situ* stomach content (~21%; Le  
609 Luherne, 2012). By contrast, the latter empirical study did not show the presence of southern  
610 shortfin squid in the stomach of analysed individuals. Differences between model outputs and  
611 observations may again result from differences in diet when estimated from the entire modelled  
612 domain rather than from some particular locations as in the study of Le Luherne (2012). Differences  
613 in the diet of predators may also result from inter- annual variations in the spatial distribution and  
614 density of prey. Furthermore, a major bias in the modelling of the diet of Atlantic horse mackerel  
615 adults is that a dominant proportion of consumed prey (~54% of macrozooplankton in the form of  
616 pteropods and ~21% of decapods, Le Luherne, 2012) is not represented as potential prey in the  
617 model.  
618 In the model, the juveniles of Atlantic mackerel (<20 cm) mainly consume certain planktivorous

619 fish, a result which is consistent with observations (Le Luherne, 2012). However, the modelled diet  
620 appears to be dominated by European pilchard (~38%) and European anchovy (~22%), while the  
621 analysis of stomach content data rather shows a high consumption of sprats (~37%) and to a lesser  
622 extent, anchovies (~16%). Accessory prey are diverse (*i.e.* mesozooplankton, northern krill,  
623 southern shortfin squid, Atlantic horse mackerel, blue whiting, other prey), each of them accounting  
624 for 6 to 7% of the modelled diet. The differences in the consumed fish species between the model  
625 and observations may be attributable to differences in species composition between the modelled  
626 period (2001-2004) and the field studies that were carried out in 2011-2012 (Le Luherne, 2012).  
627 Since 2008, the biomass of European pilchard has strongly declined in the Gulf of Lions, while that  
628 of sprat has increased (Van Beveren et al., 2014). Macrozooplankton and groups of benthic species  
629 that are not represented in the model account for significant proportions of the stomach content  
630 (~27%, ~19% respectively, Le Luherne, 2012). The model succeeded in predicting the functional  
631 group consumed (*i.e.* planktivorous fish) for the juveniles of Atlantic mackerel. Adults of Atlantic  
632 mackerel (>20 cm) are even more piscivorous than juveniles, since their modelled diet is almost  
633 90% composed of fish. The most consumed fish are firstly European pilchard (~46%) and  
634 secondarily, European anchovy (~26%), in the model. Comparatively, the proportion of consumed  
635 teleosts observed in stomach content amounts to almost 90% in the study of Le Luherne (2012), but  
636 the teleost species could not be identified due to too advanced digestion of prey.

637 Juveniles of blue whiting (<15 cm) have a rather diversified diet in the model. They feed on certain  
638 plankton groups (mesozooplankton at ~19%, and northern krill at ~25%), on southern shortfin squid  
639 (~10%) and on different species of fish (~46%). The most consumed fish species are European  
640 pilchard (~27%), Atlantic horse mackerel (~10%) and blue whiting (~6%). This result is different  
641 from those obtained in the study of Bourgoigne (2013) who observed only decapods (not represented  
642 in the model) in the stomach content of analysed juveniles. In the model, adults of blue whiting  
643 (>15 cm) mainly feed on fish (~65%) secondarily on northern krill (~26%) and southern shortfin  
644 squid (~10%). The most preyed species of fish are European pilchard (~32%), Atlantic horse

645 mackerel (~11%), blue whiting (~12%) and European anchovy (~8%). The study of Bourgogne  
646 (2013) showed a proportion of northern krill (~33%) close to that provided by the model. The main  
647 difference between model and observations is in the dominant prey. The proportion of teleosts  
648 consumed amounts to ~65% in the model, while stomach content data show a lower proportion  
649 (~35%, Bourgogne, 2013). In parallel, benthic decapods (not modelled) have been found in a  
650 significant proportion (~32%) in the stomach content of analysed adults, which may explain the  
651 mismatch between the modelled diet of adults and field data.

652 In the model, the main prey of the European hake juveniles are teleosts (~90%). Among these  
653 teleosts, the most consumed species are firstly the European pilchard (~42%), secondly the  
654 European anchovy (~24%) and thirdly, the blue whiting (~13%). In parallel, a recent study of  
655 stomach content from the same area (Mellon-Duval et al., 2017) revealed *in situ* diet mainly  
656 composed of teleosts (>80% and to 100%). In more detail, the European pilchard was observed in  
657 the highest proportion (22 to 74%), but the European anchovy and the blue whiting were also  
658 detected in lesser proportions (6 to 30% and 1 to 3%, respectively). The model results also match  
659 the observations of two other recent studies, estimating at ~92% the proportion of teleosts in the  
660 diet of juveniles (Merquiol, 2016; Bănaru and Harmelin-Vivien, 2017). In the model, adults, as  
661 juveniles, feed mostly on teleosts (~93%). The teleost prey are firstly European pilchard in a  
662 proportion of ~43%, and secondly, blue whiting at ~13%. Other fish species such as European sprat,  
663 Atlantic mackerel and European hake supplement their diet up to 16%. Mellon-Duval et al. (2017)  
664 found from the analysis of stomach content a roughly similar proportion of European pilchard  
665 (~38%) and slightly higher proportion of blue whiting (~26 to ~30%).

666 The modelled diet of Atlantic Bluefin tuna is almost exclusively piscivorous (~93%) and composed  
667 of small teleosts. European pilchard is the main prey (~51%), while European anchovy (~23%) and  
668 blue whiting (~10%) are the secondary prey. Southern shortfin squid is only an accessory prey  
669 (~7%). This preference for planktivorous teleosts, mainly European anchovy, has already been  
670 shown from the analysis of the stomach content of individuals caught in the Gulf of Lions (Imbert

671 et al., 2007). Once again, the minor mismatches observed between the modelled diet and that from  
672 the field data may result from a dataset based on sampling carried out outside the temporal window  
673 of the simulation period. This fast-swimming pelagic tuna species has been shown to have a high  
674 variability in its distribution at different spatial and temporal scales in the GoL (Royer et al., 2004).

675

### 676 3.4. Comparing TL in the E2E modelled food web with literature data

677 The E2E modelled food web (Figure 8) is composed of 15 compartments organised into four  
678 trophic levels (TL). This food web length is rather common in natural ecosystems (Hastings and  
679 Conrad, 1979). Five plankton groups represent the lowest TL ([1-2]), while ten invertebrates and  
680 teleost groups represent the highest TL (>3). The highest flows of predation occur between the  
681 phyto- and zooplankton groups ( $>10^6$  tons  $y^{-1}$ ), and sharply decrease with increasing TL, which is a  
682 common feature observed in trophic pyramids (Odum, 1959). Primary producers such as nano- and  
683 microphytoplankton representing the first TL are mainly consumed by nano- (TL=2.0), micro-  
684 (TL=2.0) and mesozooplankton (TL=2.2). Among these groups, mesozooplankton has the highest  
685 TL, as it consumes both phyto- and zooplankton. Planktivorous species such as northern krill  
686 (TL=2.5), European pilchard (TL=2.7), European anchovy (TL=2.8) and European sprat (TL=2.9)  
687 mainly feed on micro- and mesozooplankton. The European pilchard has a more omnivorous diet,  
688 with a consumption of microphytoplankton of the same order of magnitude as that of  
689 microzooplankton, or even higher than that of mesozooplankton. For these planktivorous species,  
690 TL increases from the northern krill to the European sprat, in agreement with literature data  
691 (Båmstedt and Kjørstøl, 1998; Stergiou and Karpouzi, 2002; Le Bourg et al., 2015).

692 Among the meso-predators, the Atlantic horse mackerel has the lowest TL (TL=3.5), followed by  
693 those of Atlantic mackerel (TL=3.9), southern shortfin squid (TL=4.0), blue whiting (TL=4.0),  
694 Atlantic bluefin tuna (TL=4.0) and European hake (TL=4.1). These TLs are close to field data  
695 (Stergiou and Karpouzi, 2002; Sara and Sarda, 2007; Bănară, 2015; Bănară and Harmelin-Vivien,  
696 2017; Mellon-Duval et al., 2017). Some larvae of these teleosts are consumed by cannibalism and

697 also by other species of similar, lower and higher TL.

698 On the whole, the modelled TLs are in agreement with literature data and ECOPATH-GoL outputs  
699 for most of the 10 HTL species (Figure 9). Some interesting points can however be highlighted. The  
700 modelled TLs of southern shortfin squid are slightly higher than those in the literature (Bănanu et  
701 Harmelin-Vivien, 2017) and from ECOPATH outputs (Bănanu et al., 2013). The predator-prey size  
702 ratios of the present model may be better adjusted in order to obtain a modelled TL for southern  
703 shortfin squid closer to field and literature data.

704 The modelled TLs of juveniles and adults of European pilchard are close to the minimum values  
705 estimated from the analysis of the stomach content (Stergiou and Karpouzi, 2002) or using  $\delta^{15}\text{N}$   
706 stable isotope ratios (Bănanu, 2015), while the corresponding larvae show their numerical TLs close  
707 to the observed highest values. In this case too, the predator-prey size ratios of the model may be  
708 better adjusted.

709 The TLs of all species (except pilchard, and to a lesser extent blue whiting) increase with increasing  
710 size of individuals. In order to better account for ontogenetic changes in TL (Chassot et al. 2008;  
711 Reed et al. 2017), it would be useful in the future to better refine field estimation of trophic levels  
712 by size.

713 It is interesting and encouraging to note that the TLs computed from two very different approaches  
714 of E2E modelling (*i.e.* OSMOSE *vs.* ECOPATH) are very close for most of HTL species, except for  
715 European pilchard and blue whiting. Even if the represented periods in these models partly overlap  
716 (2001-2004 for OSMOSE and 2000-2009 for ECOPATH) and the modelled area is the same, major  
717 differences in conception between these two models (opportunistic, size-based diet in OSMOSE  
718 and fixed diet in ECOPATH) may explain these small differences in trophic level results. OSMOSE  
719 is an individual size-based, spatial and dynamic model, while ECOPATH is a mass-balanced model,  
720 with no size groups, non-spatialized and offering a static snapshot of the system. Moreover,  
721 ECOPATH includes more groups and species (benthic groups, marine mammals, birds and others),  
722 which are not represented in OSMOSE. Data gaps concerning the diet of some species were

723 highlighted by Bănaru et al. (2013), and new recent diet data were included in the OSMOSE model  
724 parametrization.

725

#### 726 **4. Conclusion**

727 The GoL is a highly exploited area for fisheries (Demaneche et al., 2009; Bănaru et al., 2013). Here,  
728 as in other parts of the world, fishing has reduced the biomass of top predators (Aldebert, 1997;  
729 Piroddi et al., 2017), with potential cascading effects on the flows and biomass in the food web  
730 (Pily et al., 1998; Cury et al., 2003; Bănaru et al., 2010; Ferretti et al., 2010). Climate variations  
731 impact the GoL ecosystems through river inputs (Ludwig et al., 2009) or hydrological processes  
732 (Hermann et al., 2008). As shown in other areas, the impact of fishing combined with climate  
733 changes induces sometimes unexpected effects in the ecosystems (Travers-Trolet et al., 2014; Auber  
734 et al., 2015). The end-to-end modelling approach aims at understanding and anticipating some of  
735 these processes.

736 This paper presents the first spatialized dynamic coupled end-to-end ecosystem model for the GoL.  
737 The modeled groups and species represent more than 70% of annual catches in this area, and they  
738 encompass the pelagic and demersal ecosystem trophic structure organised into four trophic levels.  
739 The assessment of both LTL and HTL groups and species of the E2E OSMOSE-GoL model showed  
740 a satisfactory agreement with literature, satellite and field local data in terms of biomass, landings  
741 and diet. The model has been parametrized with the best available local data. Following the  
742 calibration stage, realistic ranges for the biomass and landings have been obtained for most species  
743 and groups. Biomass for the European hake and landings for the Atlantic mackerel are however  
744 slightly overestimated. At first sight, it might be considered that these differences are acceptable  
745 owing to uncertainties existing in biomass estimations and landings data. However, some  
746 improvements of the model are obviously still possible. Predator-prey size ratios may be refined to  
747 produce a better correspondence between model and field data. Sex-ratio established by default at  
748 0.5 may be refined with field data when available. The distribution maps currently based on

749 presence-absence may be replaced with density-based maps. Fishing mortality considered uniform  
750 for the entire domain may be also spatialized.

751 Previous versions of the OSMOSE model have already been applied in different ecosystems to  
752 address various questions regarding: i/ the assessment of the ecosystem trophic structure (Marzloff  
753 et al., 2009; Grüss et al., 2015; Houchi et al., 2016, Fu et al., 2017), ii/ the effect of Marine  
754 Protected Areas (Yemane et al., 2009), iii/ the combined effects of fishing and climate change  
755 (Travers et al., 2009; Fu et al., 2013; Travers-Trolet et al., 2014; Fu et al., 2018) iv/ the simulation  
756 of fishing scenarios (Shin et al., 2004; Travers et al., 2010; Smith et al., 2011; Grüss et al., 2016),  
757 and v/ the testing of indicator performance (Travers et al., 2006; Shin et al., 2018). However, the  
758 present version of E2E OSMOSE for the GoL may go further, in the analysis of the fine impact of  
759 the predation pressure exerted by HTL planktivorous species on the spatial distributions and the  
760 structure (size, trophic shortcut, *etc.*) of the plankton community. It may also contribute to the  
761 understanding of complex processes of simultaneous bottom-up and top-down controls in this  
762 exploited ecosystem (Diaz et al., 2019). Moreover, this type of E2E model may allow for the  
763 quantitative assessment of the combined effects of fishing and climate change scenarios on the  
764 ecosystem dynamics and for the computation of model-based indicators used to assess whether an  
765 ecosystem and its services are used sustainably, and then maintained (Coll *et al.*, 2015). The impact  
766 of existing or future Marine Protected Areas (Gulf of Lions, Fisheries Restricted Area, *etc.*) and  
767 spatio-temporal management measures on the structure and the functioning of the ecosystem may  
768 also be tested in future.

769 This coupled E2E model may be extended to the entire Mediterranean Sea and compared with  
770 existing Ecopath with Ecosim ecosystem model configurations (Coll and Liberto, 2012; Piroddi et  
771 al., 2017).

772

773 **Acknowledgements**

774 This study was funded by the project EMIBIOS (End-to-end Modelling and Indicators for.  
775 BIODiversity Scenarios, FRB contract no. APP-SCEN-2010-II) and by the EU FP7 project  
776 PERSEUS (Policy-oriented marine Environmental Research for the Southern European Seas,  
777 Theme “Oceans of Tomorrow” OCEAN.2011-3 Grant Agreement No. 287600). It benefited from  
778 and contributed to MERMEX WP2 collaborative work and to the MERMEX IPP “Interactions  
779 plancton-planctonophages” project. We wish to thank J.M. Fromentin, J.L. Bigot, C. Saraux, A.  
780 Jadaud for providing some data and expertise. The authors acknowledge T. Ballerini for her  
781 contribution to the coupling code and suggestions that improved the parametrization of the  
782 OSMOSE-GoL model, the assistance of staff maintaining the clusters DATARMOR of the  
783 IFREMER and HPC Platform of the OSU Institut PYTHEAS (Aix-Marseille University, INSU-  
784 CNRS) for providing the computing facilities, as well as for technical assistance. Thanks are also  
785 addressed to Michael Paul for English corrections.

786

## 787 **References**

788

789 Aldebert, Y., 1997. Demersal resources of the Gulf of Lions (NW Mediterranean). Impact of  
790 exploitation on fish diversity. *Vie et Milieu* 47, 275–285.

791 Auber, A., Travers-Trolet, M., Villanueva, M.C., Ernande, B., 2015. Regime Shift in an Exploited  
792 Fish Community Related to Natural Climate Oscillations. *PLoS ONE* 10(7), e0129883.  
793 <https://doi.org/10.1371/journal.pone.0129883>.

794 Auger, P., Diaz, F., Ulses, C., Estournel, C., Neveux, J., Joux, F., Pujo-Pay, M., Naudin J.-J., 2011.  
795 Functioning of the planktonic ecosystem on the Gulf of Lions shelf (NW Mediterranean)  
796 during spring and its impact on the carbon deposition: A field data and 3-D modelling  
797 combined approach. *Biogeosciences* 8(11), 3231–3261. doi:10.5194/bg-8-3231-2011.

798 Auger, P.-A., Ulses, C., Estournel, C., Stemmann, L., Somot, S., Diaz, F., 2014. Interannual control  
799 of plankton ecosystem in a deep convection area as inferred from a 30-year 3D modelling

800 study: winter mixing and prey/predator interactions in the NW Mediterranean. *Prog.*  
801 *Oceanogr.* 124, 12-27. doi.org/10.1016/j.pocean.2014.04.004.

802 Baklouti, M., Diaz, F., Pinazo, C., Faure, V., Quéguiner, B., 2006a. Investigation of mechanistic  
803 formulations depicting phytoplankton dynamics for models of marine pelagic ecosystems and  
804 description of a new model. *Progr. Oceanogr.* 71, 1–33. doi:10.1016/j.pocean.2006.05.002.

805 Baklouti, M., Faure, V., Pawlowski, L., Sciandra, A., 2006b. Investigation and sensitivity analysis  
806 of a mechanistic phytoplankton model implemented in a new modular numerical tool  
807 (Eco3M) dedicated to biogeochemical modelling. *Progr. Oceanogr.* 71, 34–58.  
808 doi:10.1016/j.pocean.2006.05.003.

809 Båmstedt, U., Karlson, K., 1998. Euphausiid predation on copepods in coastal waters of the  
810 Northeast Atlantic. *Mar. Ecol. Progr. Ser.* 172, 149-168. doi: 10.3354/meps172149.

811 Bănaru, D., 2015. Pelagic and demersal foodweb of the Gulf of Lions elucidated by stable isotope  
812 analysis. *MERMEX WP2, MISTRALS Workshop, Marseille, 20-22 octobre 2015.*

813 Bănaru, D., Harmelin-Vivien, M., 2017. Résultats DCSMM obtenus lors des campagnes MEDITS  
814 et PELMED 2015 sur la façade Méditerranéenne ». Dans Mialet et al., 2017. Bilan des essais  
815 et optimisation du suivi mutualisé « réseaux trophiques et contaminants » sur les campagnes  
816 halieutiques DCF 2014-2015. Programmes de surveillance DCSMM « Poissons et  
817 Céphalopodes, contaminants, questions sanitaires » sur les plateaux continentaux, 112 pp (In  
818 French).

819 Bănaru, D., Harmelin-Vivien, M., Boudouresque, C.-F., 2010. Man-induced change in community  
820 control in the north-western Black Sea: the top-down bottom-up balance. *Mar. Environ. Res.*  
821 69(4), 262-275. doi: 10.1016/j.marenvres.2009.11.009.

822 Bănaru, D., Mellon-Duval, C., Roos, D., Bigot, J.-L., Souplet, A., Jadaud, A., Beaubrun, P.,  
823 Fromentin, J.-M., 2013. Trophic structure in the Gulf of Lions marine ecosystem (North-  
824 Western Mediterranean Sea) and fishing impacts. *J. Mar. Syst.* 111-112, 45-68. doi :  
825 10.1016/j.jmarsys.2012.09.010.

826 Bode, A., Álvarez-Ossorio, M.T., Carrera, P., Lorenzo, J., 2004. Reconstruction of trophic pathways  
827 between plankton and the North Iberian sardine (*Sardina pilchardus*) using stable isotopes.  
828 Sci. Mar. 68, 165-178. doi.org/10.3989/scimar.2004.68n1165.

829 Borne, D., Tirelli, V., Brandt, S.B., Fonda Umani, S., Arneri, E., 2009. Diet of *Engraulis*  
830 *encrasicolus* in the northern Adriatic Sea (Mediterranean): ontogenetic changes and feeding  
831 selectivity. Mar. Ecol. Prog. Ser. 392, 193-209. doi: 10.3354/meps08214.

832 Bosc, E., Bricaud, A., Antoine, D., 2004. Seasonal and interannual variability in algal biomass and  
833 primary production in the Mediterranean Sea, as derived from 4 years of SeaWiFS  
834 observations. Global Biogeochemical Cycles 18(1), 1-17. doi:10.1029/2003GB002034.

835 Bourgogne, H., 2013 Etude de la stratégie alimentaire du *Micromesistius poutassou* (Risso, 1827)  
836 dans le golfe du Lion (France). Rapport de stage Master 1 Océanographie, Aix-Marseille  
837 Université, 8 pp.

838 Bricaud, A., Babin, M., Claustre, H., Ras, J., Tièche, F., 2010. Light absorption properties and  
839 absorption budget of southeast pacific waters. J. Geophys. Res. 115, C08009.  
840 doi.org/10.1029/2009JC005517.

841 Bundy, A., 2004. Mass balance models of the eastern Scotian Shelf before and after the cod collapse  
842 and other ecosystem changes. Can. Tech. Rep. Fish. Aquat. Sci. 2520, 1488-5379.

843 Campbell, R., Diaz, F., Hu, Z., Doglioli, A., Petrenko, A., Dekeyser, I., 2013. Nutrients and  
844 plankton spatial distributions induced by a coastal eddy in the Gulf of Lion. Insights from a  
845 numerical model. Progr. Oceanogr. 109, 47-69. doi.org/10.1016/j.pocean.2012.09.005.

846 Campillo, A., 1992. Les pêcheries françaises de Méditerranée: synthèse des connaissances.  
847 IFREMER RI DRV 92-019 RH/Sete. ([http://archimer.ifremer.fr/doc/00000/1125/.](http://archimer.ifremer.fr/doc/00000/1125/)) 206 pp.

848 Carlotti, F., Eisenhauer, L., Campbell, R., Diaz, F., 2014. Modelling spatial and temporal population  
849 dynamics of the Copepod *Centropages typicus* in the North western Mediterranean Sea during  
850 the year 2001 using a 3D ecosystem model. J. Mar. Syst. 135, 97-116. doi:  
851 10.1016/j.jmarsys.2013.11.007.

852 Chassot, E., Rouyer, T., Trenkel, V.M., Gascuel D., 2008. Investigating trophic-level variability in  
853 Celtic Sea fish predators. *J.Fish Biol.* 73, 763-781. Doi: 10.1111/j.1095-8649.2008.01938.x.

854 Christensen, V., Walters, C.J., 2011. Progress in the use of modeling for fisheries management. In  
855 *Ecosystem Approaches to Fisheries: A Global Perspective*, Eds. Christensen, V., Maclean, J.  
856 L., Cambridge University Press. 189-205.

857 Coll, M., Libralato, S., 2012. Contributions of food web modelling to the ecosystem approach to  
858 marine resource management in the Mediterranean Sea. *Fish and Fisheries* 13, 60-88.  
859 doi.org/10.1111/j.1467-2979.2011.00420.x.

860 Coll, M., Piroddi, C., Albouy, C., Ben Rais Lasram, F., Cheung, W.W.L., Christensen, V., Karpouzi,  
861 V.S., Guilhaumon, F., Mouillot, D., Paleczny, M., Palomares, M.L., Steenbeek, J., Trujillo, P.,  
862 Watson, R., Pauly, D., 2012. The Mediterranean Sea under siege: spatial overlap between  
863 marine biodiversity, cumulative threats and marine reserves. *Global Ecol. Biogeogr.* 21, 465-  
864 480. doi.org/10.1111/j.1466-8238.2011.00697.x.

865 Coll, M., Shannon, L.J., Kleisner, K.M., Juan-Jordá, M.J., Bundy, A., Akoglu, A.G., Bănaru, D.,  
866 Boldt, J.L., Borges, M.F., Cook, A., Diallo, I., Fu, C., Fox, C., Gascuel, D., Gurney, L.G.J.,  
867 Hattab, T., Heymans, J.J., Jouffre, D., Knight, B.R., Kucukavsar, S., Large, S.I., Lynam, C.,  
868 Machias, A., Marshall, K.N., Masski, H., Ojaveer, H., Piroddi, C., Tam, J., Thiao, D., Thiaw,  
869 M., Torres, M.A., Travers-Trolet, M., Tsagarakis, K., Tuck, I., van der Meeren, G.I., Yemane,  
870 D., Zador, S.G., Shin, Y.-J., 2016. Ecological indicators to capture the effects of fishing on  
871 biodiversity and conservation status of marine ecosystems. *Ecol. Indic.* 60: 947-962.  
872 doi:10.1016/j.ecolind.2015.08.048.

873 Collie, J.S., Botsford, L.W., Hastings, A., Kaplan, I.C., Largier, J.L., Livingston, P.A., Plaganyi, E.,  
874 Rose, K.A., Wells, B.K., Werner, F.E., 2016. Ecosystem models for fisheries management:  
875 finding the sweet spot. *Fish and Fisheries* 1-25. doi: 10.1111/faf.12093.

876 Cotté, C., d'Ovidio, F., Chaigneau, A., Lèvy, M., Taupier-Letage, I., Mate, B., Guinet, C., 2011.  
877 Scale-dependent interactions of Mediterranean whales with marine dynamics. *Limnol.*  
878 *Oceanogr.* 56(1), 219-232. doi:10.4319/lo.2011.56.1.0219.

879 CRPMEM PACA, 2016. Etat des lieux et caractérisation de la pêche maritime et des élevages  
880 marins en PACA, 110 pp (In French).

881 Cury, P., Shannon, L., Shin, Y.J., 2003. The functioning of marine ecosystems: a fisheries  
882 perspective. In: Sinclair, M., Valdimarsson, G. Eds. *Responsible fisheries in the marine*  
883 *ecosystem* 103-124.

884 Dalsgaard, A.J.T., Pauly, D., Okey, T.A., 1997. Preliminary mass-balance model of Prince William  
885 Sound, Alaska, for the pre-spill period, 1980-1989. *Fish. Centre Res. Rep.* 5(2), 1-34. doi:  
886 10.14288/1.0074775.

887 Demaneche, S., Merrien, C., Berthou, P., Lespagnol, P., 2009. Rapport R3 Méditerranée  
888 continentale, échantillonnage des marées au débarquement. Méthode d'élévation et évaluation  
889 des captures et de l'effort de pêche des flottilles de la façade Méditerranée continentale sur la  
890 période 2007-2008. Programme P6 AESYPECHE "Approche écosystémique de l'halieutique"  
891 Projet Système d'Informations Halieutiques SIH, IFREMER, France, 54 pp (In French).

892 Diaz, F., Bănar, D., Verley, P., Shin, Y., 2019. Implementation of an end-to-end model of the Gulf  
893 of Lions ecosystem (NW Mediterranean Sea). II. Investigating the effects of high trophic  
894 levels on nutrients and plankton dynamics and associated feedbacks. *Ecol. Modell.* 405, 51-  
895 68. doi: 10.1016/j.ecolmodel.2019.05.004

896 Dickmann, M., 2005. Feeding ecology of sprat (*Sprattus sprattus* L.) and sardine (*Sardina*  
897 *pilchardus* W.) larvae in the Baltic Sea and in the North Sea. PhD report Rostock University,  
898 93 pp.

899 D'Ortenzio, F., Ribera d'Alcalà, M., 2009. On the trophic regimes of the Mediterranean Sea: a  
900 satellite analysis. *Biogeosciences* 6, 139-148. <https://doi.org/10.5194/bg-6-139-2009>.

- 901 Dufau-Julliand, C., Marsaleix, P., Petrenko, A.A., Dekeyser I., 2004. Three-dimensional modelling  
902 of the Gulf of Lion's hydrodynamics (northwest Mediterranean) during January 1999  
903 (MOOGLI3 Experiment) and late winter 1999: Western Mediterranean Intermediate Water's  
904 (WIW's) formation and its cascading over the shelf break. *J. Geophys. Res.* 109, C11002. doi:  
905 10.1029/2003JC002019.
- 906 Farrugio, H., Alvarez Prado, F., Lleonart, J., De Ranieri, S., 1991. Etude pour l'aménagement et la  
907 gestion des pêches en Méditerranée occidentale. Rapport final Commission des Communautés  
908 Européennes, Contrat no. MA-1-232, 454 pp (In French).
- 909 Ferretti, F., Worm, B., Britten, G.L., Heithaus, M.R., Lotze, H.K., 2010. Patterns and ecosystem  
910 consequences of shark declines in the ocean. *Ecol. Lett.* 13, 1055–1071. doi:10.1111/j.1461-  
911 0248.2010.01489.x.
- 912 Fromentin, J.M., Farrugio, H., Deflorio, M., De Metrio, G., 2003. Preliminary results of aerial  
913 surveys of bluefin tuna in the Western Mediterranean sea. *Col. Vol. Sci. Pap. ICCAT* 55(3),  
914 1019-1027.
- 915 Fu, C., Perry, I., Shin, Y.-J., Schweigert, J., Liu, H., 2013. An ecosystem modelling framework for  
916 incorporating climate regime shifts into fisheries management. *Progr. Oceanogr.* 115, 53–64.  
917 doi:10.1016/j.pocean.2013.03.003.
- 918 Fu, C., Olsen, N., Taylor, N., Grüss, A., Batten, S., Liu, H., Verley, P., Shin, Y.-J., 2017. Spatial and  
919 temporal dynamics of predator-prey species interactions off western Canada. *ICES J. Mar.*  
920 *Sci.* 74 (8), 2107-2119. doi.org/10.1093/icesjms/fsx056.
- 921 Fu, C., Travers-Trolet, M., Velez, L., Grüss, A., Bundy, A., Shannon, L.J., Fulton, E.A., Akoglu, E.,  
922 Houle, J.E., Coll, M., Verley, P., Heymans, J.J., John, E., Shin, Y.-J. 2018. Risky business: the  
923 combined effects of fishing and changes in primary productivity on fish communities. *Ecol.*  
924 *Modell.* 368, 265-276. doi.org/10.1016/j.ecolmodel.2017.12.003.

925 Gernez, P., Antoine, D., Huot, Y., 2011. Diel cycles of the particulate beam attenuation coefficient  
926 under varying trophic conditions in the northwestern Mediterranean Sea: Observations and  
927 modeling. *Limnol. Oceanogr.* 56(1), 17-36. doi: 10.4319/lo.2011.56.1.0017.

928 GFCM-FAO, 2011a. Report of the SCSA working group on stock assessment of small pelagic  
929 species, Campobello di Mazara, Italy, 1-6 November 2010.

930 GFCM-FAO, 2011b. Report of the working group on stock assessment of small pelagics species,  
931 Chania, Greece, 24-29 october 2011.

932 Gifford, D.J., Caron, D.A., 1999. Sampling, preservation, enumeration and biomass of marine  
933 protozooplankton. In: Harris, R.P., Wiebe, P.H., Lenz, J., Skjoldal, H.R., Huntley, M. (eds)  
934 ICES Zooplankton Methodology Manual. Academic Press, London, 193-221.

935 Gregg, W.W., Casey, N.W., 2004. Global and regional evaluation of the SeaWiFS chlorophyll data  
936 set. *Remote Sens. Environ.* 93, 463-479. doi:10.1016/j.rse.2003.12.012.

937 Grüss, A., Schirripa, M.J., Chagaris, D., Drexler, M., Simons, J., Verley, P., Shin, Y.-J., Karnauskas,  
938 M., Oliveros-Ramos, R., Ainsworth, C.H., 2015. Evaluation of the trophic structure of the  
939 West Florida Shelf in the 2000s using the ecosystem model OSMOSE. *J. Mar. Syst.* 144, 30–  
940 47. doi: 10.1016/j.jmarsys.2014.11.004.

941 Grüss, A., Schirripa, M.J., Chagaris, D., Velez, L., Shin, Y.-J., Verley, P., Oliveros-Ramos, R.,  
942 Ainsworth, C.H., 2016. Estimating natural mortality rates and simulating fishing scenarios for  
943 Gulf of Mexico red grouper (*Epinephelus morio*) using the ecosystem model OSMOSE-WFS.  
944 *J. Mar. Syst.* 154, 264–279. doi:10.1016/j.jmarsys.2015.10.014.

945 Halouani, G., Ben Rais Lasram, F., Shin Y.-J., Velez, L., Verley, P., Hattab, T., Oliveros-Ramos, R.,  
946 Diaz, F., Ménard, F., Baklouti, M., Guyennon, A., Romdhane, M.S., Le Loc'h, F., 2016.  
947 Modelling food web structure using an End-to-End approach in the coastal ecosystem of the  
948 Gulf of Gabes (Tunisia). *Ecol. Modell.* 339, 45-57. doi:10.1016/j.ecolmodel.2016.08.008.

949 Hårdsted-Roméó, M., 1982. Some aspects of the chemical composition of plankton from the NW  
950 Mediterranean Sea. *Mar. Biol.* 70, 229-236.

951 Hastings, H.M., Conrad, M., 1979. Length and evolutionary stability of food chains. *Nature* 282,  
952 838.

953 Helbing, D., Brockmann, D., Chadeaux, T., Donnay, K., Blanke, U., Woolley-Meza, O., Moussaid,  
954 M., Johansson, A., Krause, J., Schutte, S., Perc, M., 2015. Saving human lives: What  
955 complexity science and information systems can contribute? *J. Stat. Phys.* 158, 735-781.  
956 <http://dx.doi.org/10.2139/ssrn.2390049>.

957 Hermann M., Estournel C., Déqué M., Marsaleix P., Sevaut F., Somot S., 2008. Dense water  
958 formation in the Gulf of Lions shelf: Impact of atmospheric interannual variability and  
959 climate change. *Cont. Shelf Res.* 28 (15), 2092-2112.  
960 <https://doi.org/10.1016/j.csr.2008.03.003>.

961 Higginbottom, R., Hosie, G.W., 1989. Biomass and population structure of a large aggregation of  
962 krill near Prydz Bay, Antarctica. *Mar. Ecol. Prog. Ser.* 58, 197-203.

963 Hu, Z.Y., Petrenko, A.A., Doglioli, A.M., Dekeyser, I., 2011a. Study of a mesoscale anticyclonic  
964 eddy in the western part of the Gulf of Lion. *J. Mar. Syst.* 88, 3-11. doi:  
965 10.1016/j.jmarsys.2011.02.008.

966 Hu, Z.Y., Petrenko, A.A., Doglioli, A.M., Dekeyser, I., 2011b. Numerical study of eddy generation  
967 in the western part of the Gulf of Lions. *J. Geophys. Res.* C12, C12030.  
968 doi:10.1029/2011JC007074.

969 Imbert, G., Bănar, D., Delord, K., Dekeyser, I., Laubier, L., 2007. Apports de l'imagerie spatiale à  
970 l'étude de la Thonaille dans les accalmies du mistral d'été. In « La Thonaille ou courantille  
971 volante » final report to Regional Provence- Alpes- Cote d'Azur Council, France, IV:117-147  
972 (In French).

973 Kaci, L., 2012. L'étude du régime alimentaire et de la forme des becs des céphalopodes dans le  
974 golfe du Lion. Stage de Licence SNTE 3ème année, Aix-Marseille Université. 31 pp (In  
975 French).

976 Kersalé, M., Petrenko, A.A., Doglioli, A.M., Dekeyser, I., Nencioli, F., 2013. Physical  
977 characteristics and dynamics of the coastal Latex09 Eddy derived from in situ data and  
978 numerical modeling. *J. Geophys. Res.* 118, 399-409. doi: 10.1029/2012JC008229.

- 979 Labat, J.-P., Cuzin-Roudy, J., 1996. Population dynamics of the krill *Meganyctiphanes norvegica*  
980 (Sars) (Crustacea: Euphausiacea) in the Ligurian Sea (NW Mediterranean Sea). Size structure,  
981 growth and mortality modelling. *J. Plankton Res.* 18: 2295-2312.
- 982 Labelle, M., Hoch, T., Liorzou, B., 1997. Analysis of the 1970-1995 bluefin sale records from  
983 french seine catches in the Mediterranean. *Col. Vol. Sci. Pap. ICCAT* 46 (2): 140-149.
- 984 Laptikhovsky, V.V., Nigmatullin, C. M., 1993. Egg size, fecundity, and spawning in females of the  
985 genus *Illex* (Cephalopoda: Ommastrephidae). *ICES J. Mar. Sci.* 50 (4), 393-403.  
986 [doi.org/10.1006/jmsc.1993.1044](https://doi.org/10.1006/jmsc.1993.1044).
- 987 Le Bourg, B., Bănaru, D., Saraux, C., Nowaczyk, A., Le Luherne, E., Jadaud, A., Bigot, J. L.,  
988 Richard, P., 2015. Trophic niche overlap of sprat and commercial small pelagic teleosts in the  
989 Gulf of Lions (NW Mediterranean Sea). *J. Sea Res.* 103, 138-146.  
990 <http://dx.doi.org/10.1016/j.seares.2015.06.011>.
- 991 Le Luherne, E., 2012. Etude de l'alimentation des maquereaux et des chinchards dans le Golfe du  
992 Lion. Rapport de stage Master 2 professionnel Environnement Marin, Aix-Marseille  
993 Université, 35 pp (In French).
- 994 Lévy, M., 2008. The modulation of biological production by oceanic mesoscale turbulence. Lecture  
995 notes in Physics, *Transport in Geophysical flow: Ten years after 744*: 219-261.
- 996 Leonart, J., 2001. Impact of fishery and environment on hake recruitment in Northwestern  
997 Mediterranean – Ilucet. EU Contract FAIR n° CT-97-3522, Final Technical Report. 680 pp.
- 998 Lotze, H.K., Coll, M., Dunne, J., 2011. Historical changes in marine resources, foodweb structure  
999 and ecosystem functioning in the Adriatic Sea. *Ecosystems* 14, 198-222.  
1000 <http://dx.doi.org/10.1007/s10021-010-9404-8>.
- 1001 Ludwig, W., Dumont, E., Meybeck, M., Heussner, S., 2009. River discharges of water and nutrients  
1002 to the Mediterranean and Black Sea: Major drivers for ecosystem changes during past and  
1003 future decades? *Progr. Oceanogr.* 80 (3-4), 199–217.  
1004 <https://doi.org/10.1016/j.pocean.2009.02.001>.

1005 Marsaleix, P., Auclair, F., Floor, J.W., Herrmann, M.J., Estournel, C., Pairaud, I., Ulses, C., 2008.  
1006 Energy conservation issues in sigma-coordinate free-surface ocean models. *Ocean Model.* 20,  
1007 61-89. doi: 10.1016/j.ocemod.2007.07.005.

1008 Marty, J.-C., Chiavérini, J., 2010. Hydrological changes in the Ligurian Sea (NW Mediterranean,  
1009 DYFAMED site) during 1995–2007 and biogeochemical consequences. *Biogeosciences* 7,  
1010 2117-2128. doi:10.5194/bg-7-2117-2010.

1011 Marty, J.-C., Chiavérini, J., Pizay, M.-D., Avril, B., 2002. Seasonal and inter-annual dynamics of  
1012 nutrients and phytoplankton pigments in the western Mediterranean Sea at the DYFAMED  
1013 time-series station (1991–1999). *Deep Sea Res. II* 49, 1965–1985. doi.org/10.1016/S0967-  
1014 0645(02)00022-X.

1015 Marzloff, M., Shin, Y.-J., Tamb, J., Travers, M., Bertrand, A., 2009. Trophic structure of the  
1016 Peruvian marine ecosystem in 2000–2006: Insights on the effects of management scenarios  
1017 for the hake fishery using the IBM trophic model Osmose. *J. Mar. Syst.* 75, 290-304.  
1018 doi:10.1016/j.jmarsys.2008.10.009.

1019 Mellon-Duval, C., de Pontual, H., Metral, L., Quemener, L., 2009. Growth of European hake  
1020 (*Merluccius merluccius*) in the Gulf of Lions based on conventional tagging. *ICES J. Mar.*  
1021 *Sci.* 67(1), 62-70. doi.org/10.1093/icesjms/fsp215.

1022 Mellon-Duval, C., Harmelin-Vivien, M., Métral, L., Loizeau, V., Mortreux, S., Roos, D., Fromentin,  
1023 J.-M., 2017. Trophic ecology of the European hake in the Gulf of Lions, northwestern  
1024 Mediterranean Sea. *Sci. Mar.* 81(1), 7-18. doi: 10.3989/scimar.04356.01A.

1025 Merquiol, L., 2016. Rapport de Master 1 sur l'alimentation et la condition du merlu européen,  
1026 *Merluccius merluccius* (L., 1758), dans le Nord-Ouest de la Méditerranée : une comparaison  
1027 2004-2015. 28 pp (In French).

1028 Millot, C., 1999. Circulation in the western Mediterranean Sea. *J. Mar. Syst.* 20 (1–4), 423–442.  
1029 doi: 10.1016/S0924-7963(98)00078-5.

- 1030 Minas, M., Minas, H.J., 1989. Primary production in the gulf of Lions with considerations to the  
1031 Rhone River input. *Water Pollution Research Reports* 13, 112-125.
- 1032 Niewiadomska, K., Claustre, H., Prieur, L., d'Ortenzio, F., 2008. Submesoscale physical-  
1033 biogeochemical coupling across the Ligurian current (northwestern Mediterranean) using a  
1034 bio-optical glider. *Limnol. Oceanogr.* 53(2), 2210–2225. doi: 10.2307/40058379.
- 1035 Odum, E.P., 1959. *Fundamentals of ecology*. Second edition. In collaboration with H.T. Odum.  
1036 Philadelphia, Saunders, XVII, 546 pp.
- 1037 Oliveros-Ramos, R., Shin, Y.-J., 2016. Calibrar: an R package for fitting complex ecological  
1038 models. *ArXiv Prepr. ArXiv160303141*.
- 1039 Oliveros-Ramos, R., Verley, P., Shin, Y.-J., 2015. A sequential approach to calibrate ecosystem  
1040 models with multiple time series data. *ArXiv Prepr. ArXiv150906123*.
- 1041 Ouillon, S., Petrenko, A., 2005. Above-water measurements of reflectance and chlorophyll-a  
1042 algorithms in the Gulf of Lions, NW Mediterranean Sea. *Opt. Express* 13, 2531-2548.  
1043 doi.org/10.1364/OPEX.13.002531.
- 1044 Palomares, M.L.D., Pauly, D., 1998. Predicting food consumption of fish populations as functions  
1045 of mortality, food type, morphometrics, temperature and salinity. *Mar. Freshw. Res.* 49 (5),  
1046 447–453. doi.org/10.1071/MF98015.
- 1047 Pauly, D., Christensen, V., Dalsgaard, A., Froese, R., Torres, J., 1998. Fishing down marine food  
1048 webs. *Science* 279 (5352), 860–863. doi: 10.1126/science.279.5352.860.
- 1049 Pethybridge, H., Bodin, N., Arsenault-Pernet, E.J., Bourdeix, J.H., Brisset, B., Bigot, J.L., Roos, D.,  
1050 Peter, M., 2014. Temporal and inter-specific variations in forage fish feeding conditions in the  
1051 NW Mediterranean: lipid content and fatty acid compositional changes. *Mar. Ecol. Prog. Ser.*  
1052 512, 39-54. doi.org/10.3354/meps10864.
- 1053 Petrenko, A., 2003. Variability of circulation features in the Gulf of Lions NW Mediterranean Sea.  
1054 Importance of inertial currents. *Oceanol. Acta* 26, 323-338. doi: 10.1016/S0399-  
1055 1784(03)00038-0.

1056 Piroddi, C., Coll, M., Liqueste, C., Macias, D., Greer, K., Buszowski, J., Steenbeek, J., Danovaro, R.,  
1057 Christensen, V., 2017. Historical changes of the Mediterranean Sea ecosystem: modelling the  
1058 role and impact of primary productivity and fisheries changes over time. *Sci. Rep.* 7, 44491.  
1059 doi:10.1038/srep44491.

1060 Quéro, J.-C., Vayne, J.-J., 1997. Les poissons de mer des pêches françaises. Eds. Delachaux Et  
1061 Niestlé, 304 pp.

1062 Reed, J., Shannon, L.J., Velez, L., Akoglu, E., Bundy, A., Coll, M., Fu, C., Fulton, E.A., Grüss, A.,  
1063 Halouani, G., Heymans, J.J., Houle, J., John, E., Le Loc'h, F., Salihoglu, B., Verley, P., Shin,  
1064 Y.-J. 2017. Ecosystem indicators – accounting for variability in species’ trophic levels. *ICES*  
1065 *J. Mar. Sci.* 74(1), 158-169. doi.org/10.1093/icesjms/fsw150.

1066 Rose, K., Allen, J.U., Artioli, Y., Barange, M., Blackford, J., Carlotti, F., Cropp, R., Daewel, U.,  
1067 Edwards, K., Flynn, K., Hill, S.L., HilleRisLambers, R., Huse, G., Mackinson, S., Megrey, B.,  
1068 Moll, A., Rivkin, R., Salihoglu, B., Schrum, C., Shannon, L., Shin, Y.-J., Smith, S.L.,  
1069 Solidoro, C., St. John, M., Zhou, M., 2010. End-To-End Models for the Analysis of Marine  
1070 Ecosystems: Challenges, Issues, and Next Steps. *Mar. Coast. Fish.* 2, 115-130.  
1071 doi.org/10.1577/C09-059.1.

1072 Rose, K., 2012. End-to-end models for marine ecosystems: Are we on the precipice of a significant  
1073 advance or just putting lipstick on a pig? *Sci. Mar.* 76(1), 195-201. doi:  
1074 10.3989/scimar.03574.20B.

1075 Ross, R.M., Quetin, L.B., 1986. How Productive are Antarctic Krill? *Bioscience* 36, 264–269.

1076 Rossi, S., Sabate, A., Latasa, S.M., Reyes, E., 2006. Lipid biomarkers and trophic linkages between  
1077 phytoplankton, zooplankton and anchovy (*Engraulis encrasicolus*) larvae in the NW  
1078 Mediterranean. *J.Plankton Res.* 28(6), 551-562. doi.org/10.1093/plankt/fbi140.

1079 Royer, F., Fromentin, J.M., Gaspar, P., 2004. Association between bluefin tuna schools and oceanic  
1080 features in the western Mediterranean. *Mar. Ecol. Prog. Ser.* 269, 249-263. doi :  
1081 10.3354/meps269249.

1082 Sacchi, J., 2008. Impact des techniques de pêche sur l'environnement en Méditerranée. GFCM  
1083 Stud. Rev. 84, 1-82.

1084 Sánchez, P., González, A.F., Jereb, P., Laptikhovsky, V.V., Mangold, K.M., Nigmatullin, Ch.M.,  
1085 Ragonese, S., 1998. *Illex coindetii*, p 18. In: FAO Fish. Tech. Pap. 376 pp.

1086 Santojanni, A., Cingolani, N., Arneri, E., Kirikwood, G., Belardinelli, A., Giannetti, G., Colella, S.,  
1087 Donato, F., Barry, C., 2005. Stock assessment of sardine (*Sardina pilchardus*, Walb.) in the  
1088 Adriatic Sea, with an estimate of discards. Sci. Mar. 69, 603-617.  
1089 doi.org/10.3989/scimar.2005.69n4603.

1090 Sara, G., Sara, R., 2007. Feeding habits and trophic levels of bluefin tuna *Thunnus thynnus* of  
1091 different size classes in the Mediterranean Sea. J. Appl. Ichthyol. 23, 122–127.  
1092 doi.org/10.1111/j.1439-0426.2006.00829.x.

1093 SCRS, 1997. Report of the ICCAT SCRS Bluefin tuna stock assessment session. Collect. Vol. Sci.  
1094 Pap. ICCAT 46(1), 1-186.

1095 Shin, Y.-J., Cury, P., 2001. Exploring fish community dynamics through size-dependent trophic  
1096 interactions using a spatialized individual-based model. Aquat. Living Resour. 14(2), 65-80.  
1097 doi.org/10.1016/S0990-7440(01)01106-8.

1098 Shin, Y.-J., Cury, P., 2004. Using an individual-based model of fish assemblages to study the  
1099 response of size spectra to changes in fishing. Can. J. Fish. Aquat. Sci. 61, 414-431.  
1100 doi.org/10.1139/f03-154.

1101 Shin, Y.-J., Shannon, L.J., Cury, P.M., 2004. Simulations of fishing effects on the southern Benguela  
1102 fish community using an individual-based model: learning from a comparison with ECOSIM.  
1103 In Ecosystem Approaches to Fisheries in the Southern Benguela. Shannon, L.J., Cochrane,  
1104 K.L. and S.C. Pillar (Eds.). Afr. J. Mar. Sci. 26, 95-114.  
1105 doi.org/10.2989/18142320409504052.

- 1106 Shin, Y.-J., Travers, M., Maury, O., 2010. Coupling models of low and high trophic levels models:  
1107 towards a pathways-orientated approach for end-to-end models. *Progr. Oceanogr.* 84, 105-  
1108 112. doi.org/10.1016/j.pocean.2009.09.012.
- 1109 Shin, Y.-J., Houle, J.E., Akoglu, E., Blanchard, J., Bundy, A., Coll, M., Demarcq, H., Fu, C., Fulton,  
1110 E.A., Heymans, J.J., Salihoglu, B., Shannon, L.J., Sporcic, M., Velez, L., 2018. The  
1111 specificity of marine ecological indicators to fishing in the face of environmental change: a  
1112 multi-model evaluation. *Ecol. Indic.* 89, 317-326.  
1113 <https://doi.org/10.1016/j.ecolind.2018.01.010>.
- 1114 Sieburth, J.McN., Jiirgen Lenx V.S., 1978. Pelagic ecosystem structure: Heterotrophic  
1115 compartments of the plankton and their relationship to plankton size fractions. *Limol.*  
1116 *Oceanogr.* 23(6), 1256-1263.
- 1117 Siegel, D.A., Doneys S.C, Yoder J.A., 2002. The North Atlantic Spring Phytoplankton Bloom and  
1118 Sverdrup's Critical Depth Hypothesis. *Science*, 296, 730-733. doi:10.1126/science.1069174.
- 1119 Sinovčić, G., Franičević, M., Zorica, B., Čikeš-Keč, V., 2004. Length-weight and length-length  
1120 relationships for 10 pelagic fish species from the Adriatic Sea (Croatia). *J. Appl. Ichthyol.*  
1121 20(2), 156-158. doi.org/10.1046/j.1439-0426.2003.00519.x.
- 1122 Smith, ADM., Brown, C.J., Bulman, C.M., Fulton, E.A., Johnson, P., Kaplan, I.C., Lozano-Montes,  
1123 H., Mackinson, S., Marzloff, M., Shannon, LJ., Shin, Y.-J., Tam, J., 2011. Impacts of fishing  
1124 low-trophic level species on marine ecosystems. *Science* 333, 1147–1150. doi:  
1125 10.1126/science.1209395.
- 1126 Stergiou, K.I., Karpouzi, V.S., 2002. Feeding habits and trophic levels of Mediterranean fish. *Rev.*  
1127 *Fish Biol. Fish.* 11 (3), 217–254.
- 1128 Travers, M., Shin, Y.-J., Jennings, S., Cury, P., 2007. Towards end-to-end models for investigating  
1129 the effects of climate and fishing in marine ecosystems. *Progr. Oceanogr.* 75 (4), 751-770.  
1130 doi.org/10.1016/j.pocean.2007.08.001.

1131 Travers, M., Shin, Y.-J., Jennings, S., Machu, E., Huggett, J.A., Field, J.G., Cury, P.M., 2009. Two-  
1132 way coupling versus one-way forcing of plankton and fish models to predict ecosystem  
1133 changes in the Benguela. *Ecol. Modell.* 220, 3089–3099.  
1134 doi:10.1016/j.ecolmodel.2009.08.016.

1135 Travers, M., Shin, Y.-J., Shannon, L.J., Cury, P., 2006. Simulating and testing the sensitivity of  
1136 ecosystem-based indicators to fishing in the southern Benguela ecosystem. *Can. J. Fish.*  
1137 *Aquat. Sci.* 63, 943-956. doi.org/10.1139/F06-003.

1138 Travers, M., Watermeyer, K., Shannon, L.J., Shin, Y.-J., 2010. Changes in food web structure under  
1139 scenarios of overfishing in the Southern Benguela: Comparison of the Ecosim and OSMOSE  
1140 modelling approaches. *J. Mar. Syst.* 79, 101-111. doi: 10.1016/j.jmarsys.2009.07.005.

1141 Travers–Trolet, M., Shin, Y.-J., Shannon, L.J., Moloney, C.L., Field, J.G., 2014. Combined Fishing  
1142 and Climate Forcing in the Southern Benguela Upwelling Ecosystem: An End-to-End  
1143 Modelling Approach Reveals Dampened Effects. *PLoS ONE* 9, e94286.  
1144 doi:10.1371/journal.pone.0094286.

1145 Ulses, C., Estournel, C., Durrieu de Madron, X., Palanques A., 2008. Suspended sediment transport  
1146 in the Gulf of Lions (NW Mediterranean): Impact of extreme storms and floods. *Cont. Shelf*  
1147 *Res.* 28, 2048-2070. <http://dx.doi.org/10.1016/j.csr.2008.01.015>.

1148 Van Beveren, E., Bonhommeau, S., Fromentin, J.M., Bigot, J.L., Bourdeix, J.H., Brosset, P., Roos,  
1149 D., Saraux, C., 2014. Rapid changes in growth, condition, size and age of small pelagic fish in  
1150 the Mediterranean. *Mar. Biol.* 161, 1809-1822. doi : 10.1007/s00227-014-2463-1.

1151 Volpe, G., Santoleri, R., Vellucci, V., Ribera d’Alcala, M., Marullo, S., D’Ortenzio, F., 2007. The  
1152 colour of the Mediterranean Sea: Global versus regional bio-optical algorithms evaluation and  
1153 implication for satellite chlorophyll estimates. *Remote Sens. Environ.* 107, 625-638. doi:  
1154 10.1016/j.rse.2006.10.017.

1155 Yemane, D., Shin, Y.-J., Field, J.G., 2009. Exploring the effect of Marine Protected Areas on the  
1156 dynamics of fish communities in the southern Benguela: an individual-based modelling  
1157 approach. *ICES J. Mar. Sci. J. Cons.* 66, 378–387. doi:10.1093/icesjms/fsn171.

1158 Walsh, J.J., 1981. A carbon budget for overfishing off Peru. *Nature* 290(5804), 300.

1159 <http://sih.ifremer.fr/>(December 2017)

1160 [www.fishbase.org](http://www.fishbase.org)

1161 [www.osmose-model.org](http://www.osmose-model.org)

1162

1163

1164 LEGENDS OF TABLES

1165

1166 **Table 1** Characteristics and parameters of the five LTL groups of the Eco3M-S model.

1167

1168 **Table 2** Parameter values of the OSMOSE-GoL model obtained from fitting the model to observed  
1169 data.  $M_0$ : intrinsic mortality rate;  $M_s$ : mortality rate due to predation from other species that are not  
1170 explicitly considered in the model;  $F$ : annual fishing mortality rate;  $a_p$ : availability coefficients of  
1171 plankton groups to HTL species.

1172

1173 **Table 3** Size classes of the different species implemented in the OSMOSE-GoL model, minimum  
1174 and maximum predator/prey size ratios. MIR= Maximum ingestion rate.

1175

1176 **Table 4** Input parameters of the OSMOSE-GoL model for each of the 10 HTL species modelled.  $K$   
1177 (growth rate),  $L_\infty$  (asymptotic size) and  $t_0$  (time at null size): the von Bertalanffy growth parameters;  
1178  $b$ : the exponent of the allometric length–weight relationship;  $c$ : constant of proportionality of the  
1179 allometric length-weight relationship;  $s_{mat}$ : size at maturity;  $\phi$ : relative fecundity;  $S$ : egg size;  $a_{max}$ :  
1180 longevity;  $s_{rec}$ : legal size of recruitment for fisheries catch.

1181

1182 **Table 5** Seasonality of the fishing activity in the GoL for target species.

1183

1184 **Table 1**

	Size range ( $\mu\text{m}$ )	Eco3M-S mortality rate, $m_p$ ( $\text{d}^{-1}$ )	Trophic level	Conversion factor ( $\text{mg}_{\text{ww}} \text{mmolN}^{-1}$ )
NANOPHY	2-20 <sup>a</sup>	0.000 <sup>b</sup>	1.0 <sup>c</sup>	993.75 <sup>d,e,f</sup>
MICROPHY	20-200 <sup>a</sup>	0.075 <sup>b</sup>	1.0 <sup>c</sup>	993.75 <sup>d,e,f</sup>
NANOZOO	5-20 <sup>a</sup>	0.043 <sup>b</sup>	1.5 <sup>c</sup>	832.50 <sup>g,h</sup>
MICROZOO	2-200 <sup>a</sup>	0.070 <sup>b</sup>	2.0 <sup>c</sup>	832.50 <sup>g,h</sup>
MESOOZOO	200-2000 <sup>a</sup>	0.033 <sup>*,b</sup>	2.5 <sup>c</sup>	150.00 <sup>**,g</sup>

1185

1186 \*Units:  $\text{m}^3 \text{mmolC}^{-1} \text{d}^{-1}$  (predation rate), \*\*Units:  $\text{mg}_{\text{ww}} \text{mmolC}^{-1}$ , <sup>a</sup>Sieburth et al. (1978), <sup>b</sup>Campbell et al. (2013),1187 <sup>c</sup>Arbitrarily set, <sup>d</sup>Dalsgaard and Pauly (1997), <sup>e</sup>Walsh (1981), <sup>f</sup>Bundy (2004), <sup>g</sup>Gifford and Caron (2000), <sup>h</sup>Hardsted-

1188 Roméo (1982).

1189

1190

1191 **Table 2**

Species	Mortality			Availability
	$M_0$	$M_s$	F	coefficients
	( $y^{-1}$ )	( $y^{-1}$ )	( $y^{-1}$ )	$a_p$
Northern krill	7.555	0.237	0.000	-
Southern shortfin squid	5.238	0.698	1.253	-
European pilchard	5.558	0.365	0.082	-
European anchovy	6.609	0.228	0.185	-
European sprat	4.549	0.404	0.000	-
Atlantic horse mackerel	1.271	0.061	0.419	-
Atlantic mackerel	9.878	0.991	0.548	-
Blue whiting	6.731	0.604	0.013	-
European hake	10.959	0.285	0.122	-
Atlantic bluefin tuna	0.000	0.000	0.642	-
NANOPHY	-	-	-	0.591
MICROPHY	-	-	-	0.223
NANOZOO	-	-	-	0.311
MICROZOO	-	-	-	0.157
MESOZOO	-	-	-	0.148

1192

1193

1194 **Table 3**

Species	Size classes (cm)	Predator/prey size ratios		MIR
		Min	Max	
	Northern krill	-	188	4
Southern shortfin squid	-	17	1	5.92
European pilchard	<3	65	13	8.0
	3-12.5	1139	15	
	>12.5	1621	60	
European anchovy	<3	500	4	4.49
	3-8	500	4	
	>8	806	7	
European sprat	<3	500	2	4.58
	3-11.6	517	10	
	>11.6	517	10	
Atlantic horse mackerel	<16	40	4	2.54
	>16	100	4	
Atlantic mackerel	<20	100	1	5.0
	>20	61	2	
Blue whiting	<15	40	3	5.92
	>15	32	4	
European hake	<36	9	1	6.76
	>36	14	1	
Atlantic bluefin tuna	-	20	4	7.95

1195

1196 **Table 4**

1197

Species	Growth					Reproduction				
	K (y <sup>-1</sup> )	L <sub>∞</sub> (cm)	t <sub>0</sub> (y)	b	c (g cm <sup>-3</sup> )	s <sub>mat</sub> (cm)	φ (egg g <sup>-1</sup> )	S (cm)	a <sub>max</sub> (y)	s <sub>rec</sub> (cm)
Northern krill	1.680	3.462	-0.2	3.16	7.38E-03	1.05	7547	0.06	1	0
Southern shortfin squid	0.930	17.400	0.087	2.12	8.96E-02	11.50	420	0.08	3	10
European pilchard	0.334	19.925	-2.164	3.25	3.8E-03	12.50	2157	0.1	7	10
European anchovy	0.609	16.29	-1.396	3.02	6.5E-03	11.00	1271	0.1	4	11
European sprat	0.370	14.20	-2.3	2.51	2.26E-02	11.40	1096	0.12	6	10
Atlantic horse mackerel	0.230	39.90	-0.94	2.84	1.3E-02	16.00	286	0.08	9	15
Atlantic mackerel	0.370	42.00	-0.50	3.13	6.7E-03	30.00	300	0.12	12	18
Blue whiting	0.230	40.50	-1.27	3.00	6.4E-03	15.00	1217	0.12	7	16
European hake	0.150	68.00	-0.47	3.03	1.0E-02	36.00	320	0.12	20	20
Atlantic bluefin tuna	0.093	318.85	-0.97	3.0092	1.96E-05	97.50	0	-	20	80

1198

1199

1200 **Table 5**

Fishing mortality / time steps	Southern shortfin squid	European pilchard	European anchovy	Atlantic horse mackerel	Atlantic mackerel	Blue whiting	European hake	Atlantic bluefin tuna
1, 2	0.042	0.024	0.048	0.026	0.042	0.017	0.014	0.000
3, 4	0.042	0.028	0.040	0.027	0.042	0.048	0.040	0.005
5, 6	0.042	0.038	0.042	0.046	0.042	0.125	0.059	0.041
7, 8	0.042	0.035	0.042	0.066	0.042	0.119	0.049	0.070
9, 10	0.042	0.044	0.050	0.062	0.042	0.113	0.057	0.052
11, 12	0.042	0.063	0.049	0.053	0.042	0.053	0.056	0.054
13, 14	0.042	0.068	0.038	0.029	0.042	0.008	0.053	0.050
15, 16	0.042	0.063	0.039	0.031	0.042	0.003	0.058	0.120
17, 18	0.042	0.052	0.046	0.048	0.042	0.004	0.055	0.096
19, 20	0.042	0.040	0.042	0.052	0.042	0.003	0.039	0.013
21, 22	0.042	0.028	0.040	0.040	0.042	0.004	0.020	0.000
23, 24	0.042	0.017	0.026	0.022	0.042	0.003	0.005	0.000

1201

1202 LEGENDS OF FIGURES

1203

1204 **Fig. 1.** Processes taken into account within each of the two models and processes linking the two  
1205 models (dashed-line arrows). The time step of Eco3M-S/SYMPHONIE (left hand side, Campbell *et*  
1206 *al.*, 2013) is one hour while that of OSMOSE (right hand side, adapted from Travers-Trolet *et al.*,  
1207 2014) is 15 days. The two-ways coupling mode is used throughout the predation process, where the  
1208 biomass of the plankton groups serve as prey field for fish schools, cephalopods and krill ("Prey  
1209 availability" arrow), while an explicit rate of HTL-induced predation is specifically applied as  
1210 feedback on each of the aforementioned five plankton groups ("Predation mortality" arrow). In the  
1211 one-way forcing mode, plankton biomasses serve as prey fields to fish schools, cephalopods and  
1212 krill ("Prey availability" arrow), without any feedback on the plankton prey compartments.

1213

1214 **Fig. 2.** The Eco3M-S/Symphonie model domain in the NW Mediterranean Sea is delineated by the  
1215 black thin line. The OSMOSE-GoL model domain over the Gulf of Lions is delimited by the black  
1216 bold line. The map of grid points in the OSMOSE-GoL domain is given in the small panel in the  
1217 right edge of the figure. The black arrow indicates the main flow of the Northern Current (NC).  
1218 Rivers taken into account by the model are named. Bathymetry with isobaths 50, 100 and 1000 m is  
1219 shown in the modeled area.

1220

1221 **Fig. 3.** Temporal patterns of change in the simulated biomass of the 10 HTL species during the last  
1222 four years of spin-up over the whole modeled domain. The solid blue line shows the median value  
1223 computed from the 50 simulation replicates. The lower and upper limits of the grey range delineate  
1224 the 0.25 and 0.75 (resp.) percentiles computed from the 50 replicates. The two horizontal dotted  
1225 black lines represent the range of observed biomass (see references 2.3).

1226

1227 **Fig. 4.** Temporal patterns of change in the simulated landings of the 10 HTL species during the last

1228 four years of spin-up over the whole modeled domain. The solid blue line shows the median value  
1229 computed from the 50 simulation replicates. The lower and upper limits of the grey range delineate  
1230 the 0.25 and 0.75 percentiles computed from the 50 simulation replicates. The horizontal black lines  
1231 represent monthly observed landings (see references 2.3).

1232

1233 **Fig. 5.** Time-series of satellite-derived (blue) and modeled (red) chlorophyll surface concentrations  
1234 ( $\text{mg m}^{-3}$ ) over the whole modeled domain. Thick lines represent mean values and shaded area (grey)  
1235 is the range of error bars computed from the GlobColour algorithm. Missing data in the time-series  
1236 are explained by cloudy days without any useable pixels.

1237

1238 **Fig. 6.** Time-series of the averaged error ( $\text{mg m}^{-3}$ ) on satellite-derived chlorophyll (blue dots) and  
1239 of the C parameter (metric of data-to-model distance in  $\text{mg m}^{-3}$ , red dots) on the whole modeled  
1240 domain.

1241

1242 **Fig. 7.** Mean diet (over the years 36 to 43) of larvae, juveniles and adults of the 10 HTL species  
1243 considered in the OSMOSE-GoL model.

1244

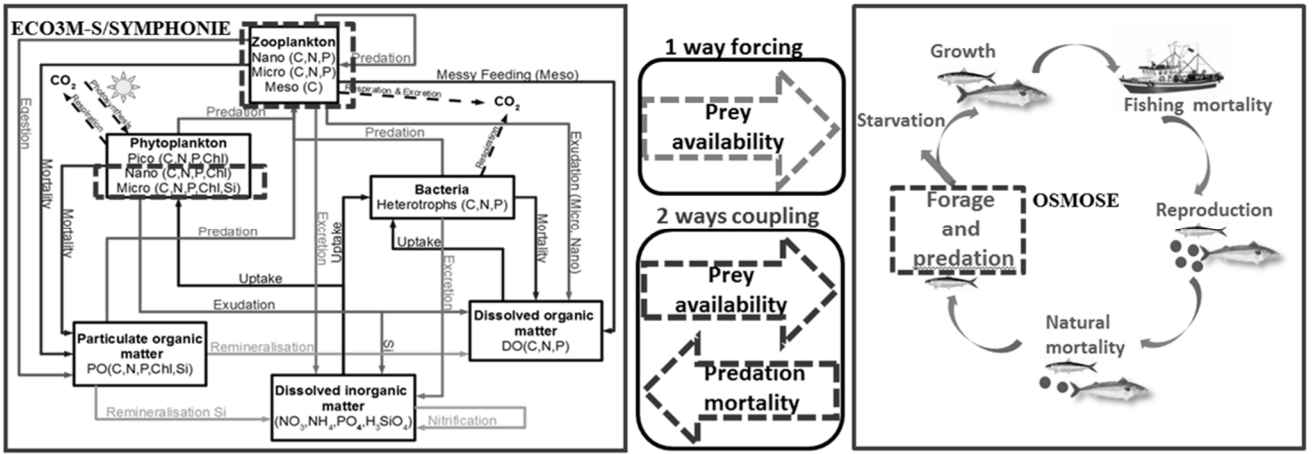
1245 **Fig. 8.** Representation of the trophic levels and the main fluxes of matter between the  
1246 compartments of the OSMOSE-GoL model (TL = trophic level, LTL = low trophic levels, HTL =  
1247 high trophic levels). Size of the arrows is related to the intensity of predation fluxes. Fluxes lower  
1248 than  $10 \text{ tons y}^{-1}$  are not quoted in the diagram. For sake of clarity, only fluxes that account for at  
1249 least 10% of predation total flux for a given prey are shown.

1250

1251 **Fig. 9.** Trophic levels vs. total length of the ten HTL species represented in the OSMOSE-GoL  
1252 model (there was a high inter-annual overlap of the trophic levels). Horizontal dashed black lines  
1253 indicate the minimum and maximum values from the literature data based on the analysis of

1254 stomach content and corresponding to a range of total length. Horizontal solid black lines indicate  
1255 the trophic levels from the ECOPATH model of the GoL (Bănaru *et al.*, 2013).  
1256

1257 Fig



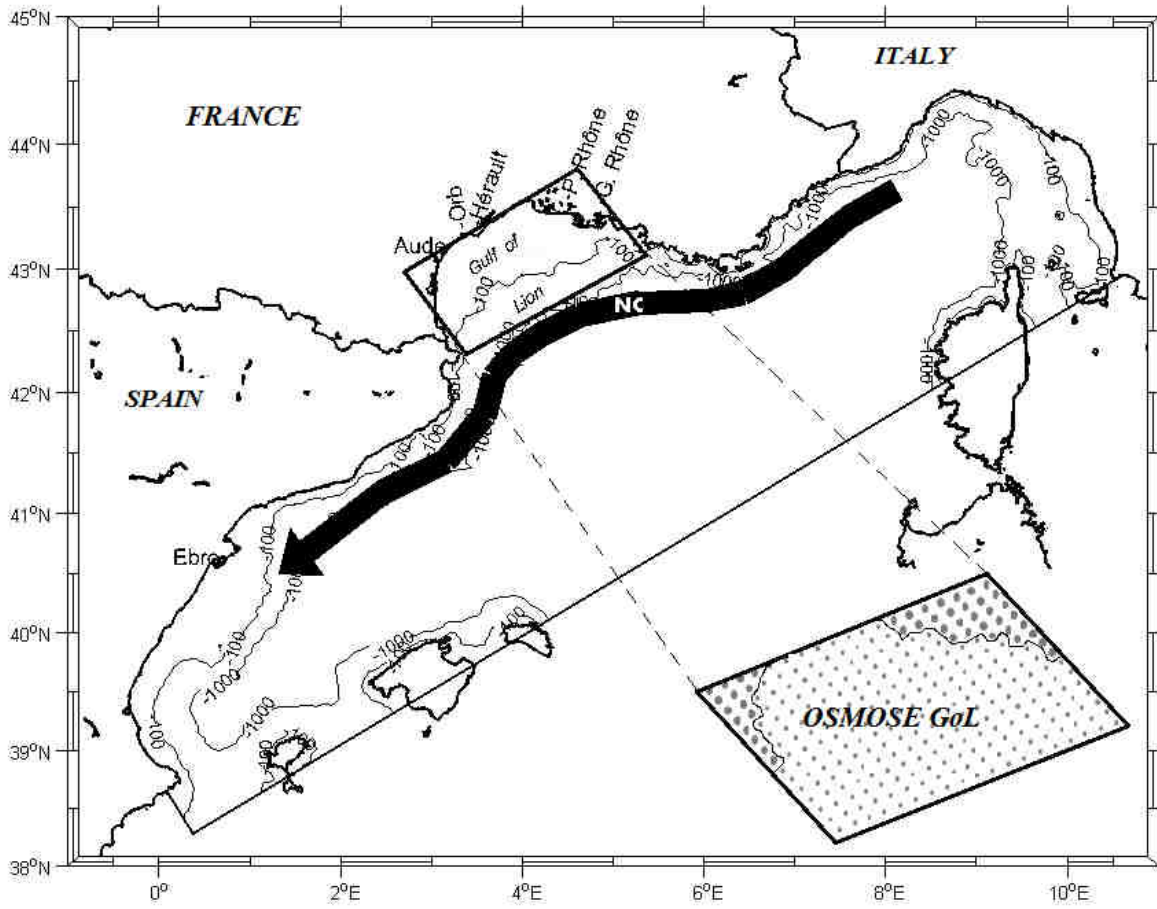
1258

1259

1260 **Fig. 2.**

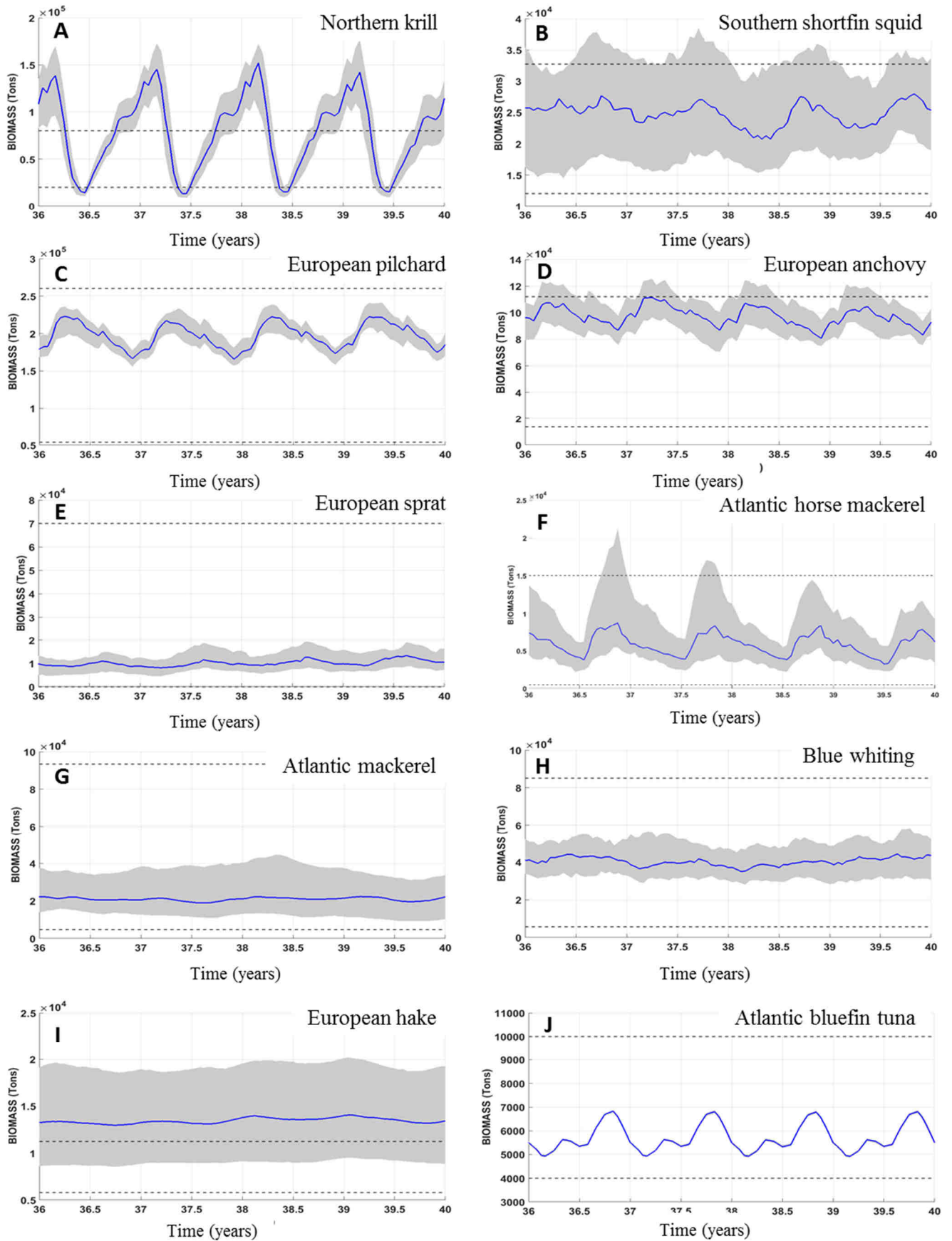
1261

1262

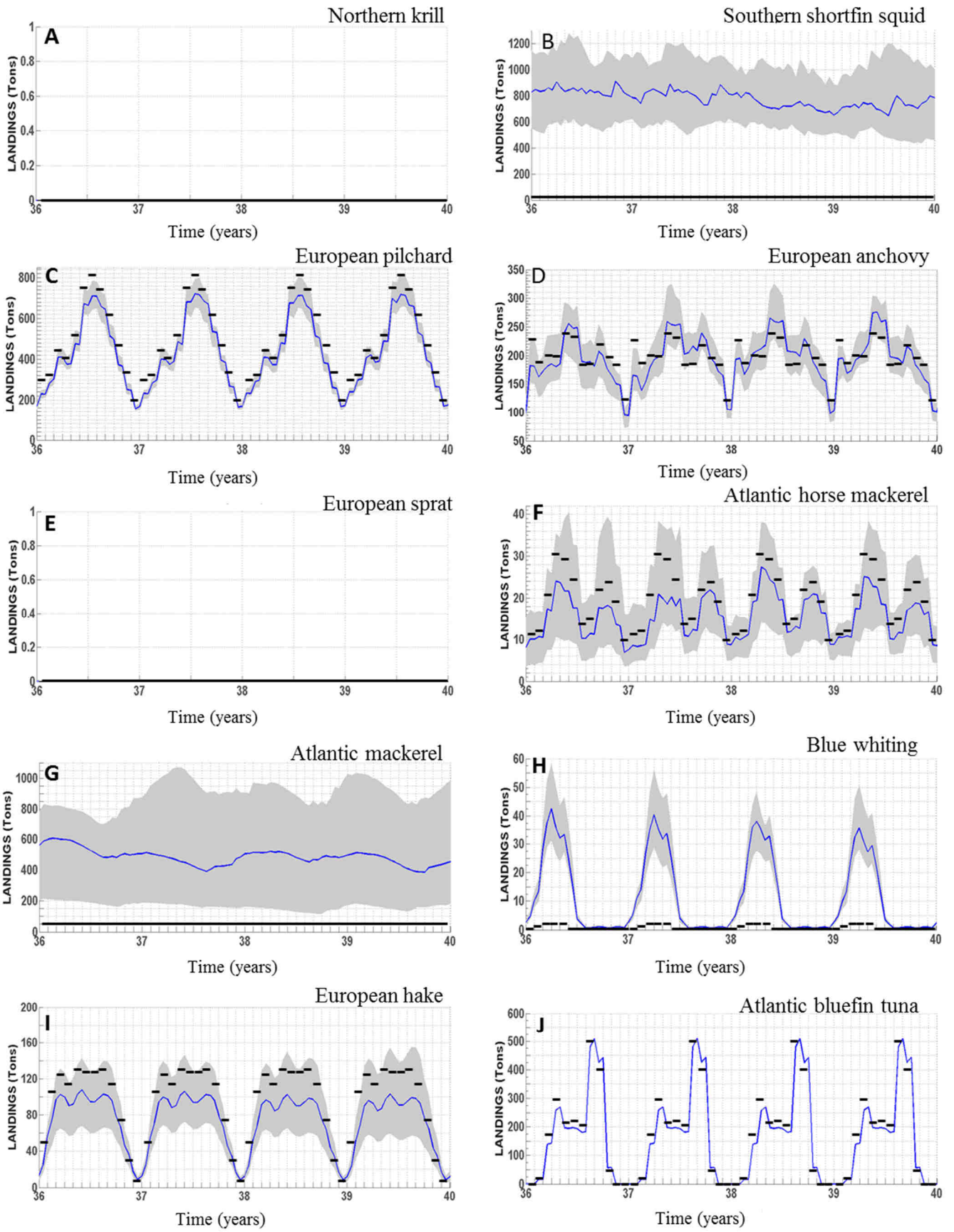


1263 Fig. 3.

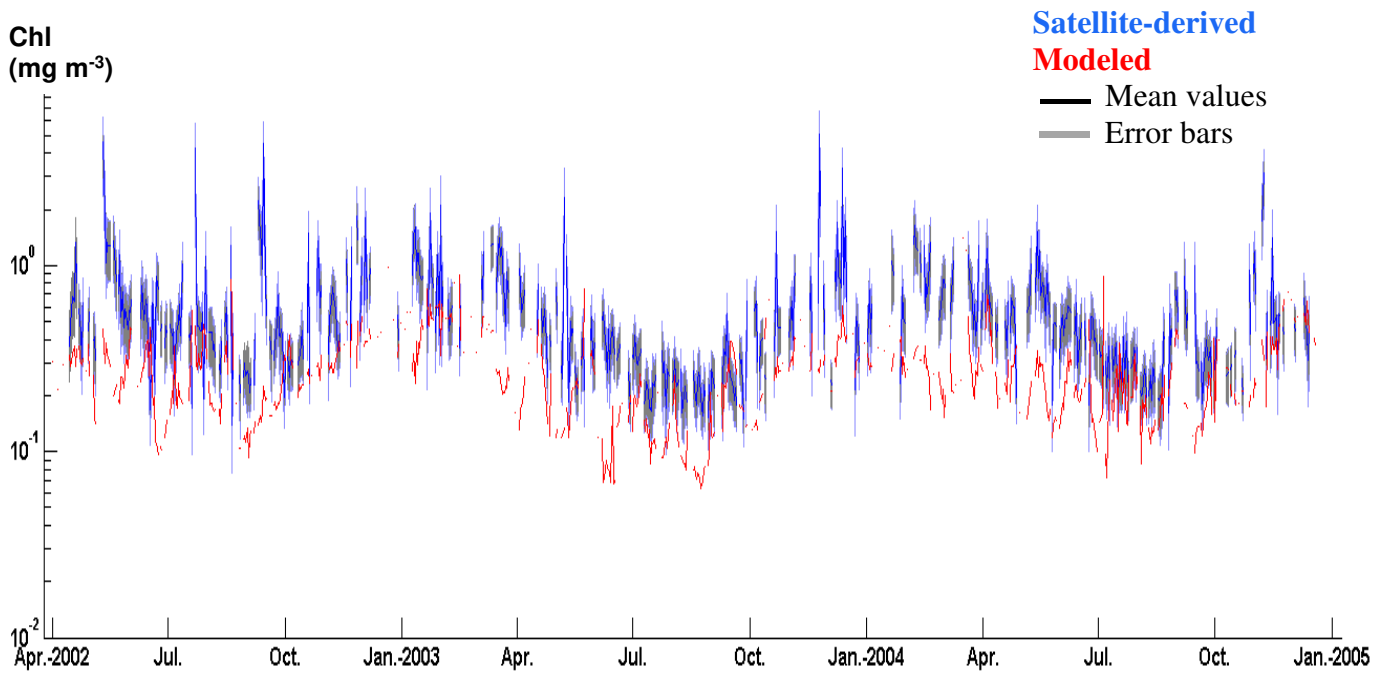
1264



1265



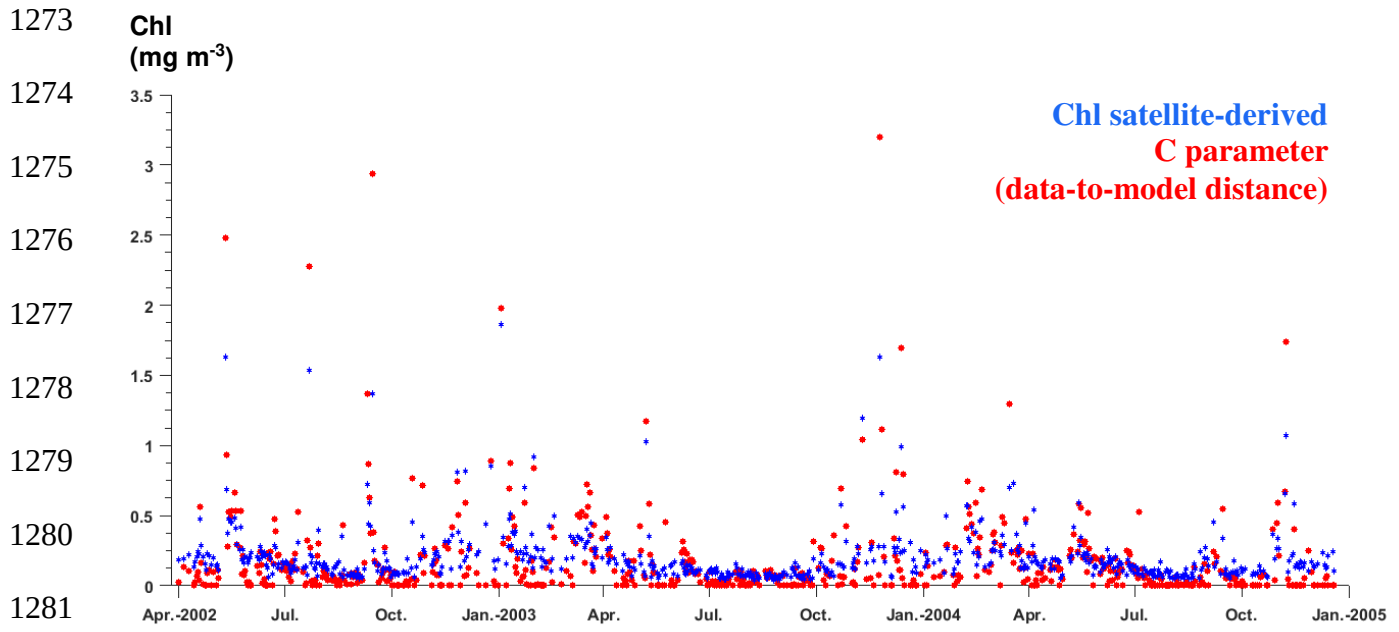
1269 **Fig. 5.**



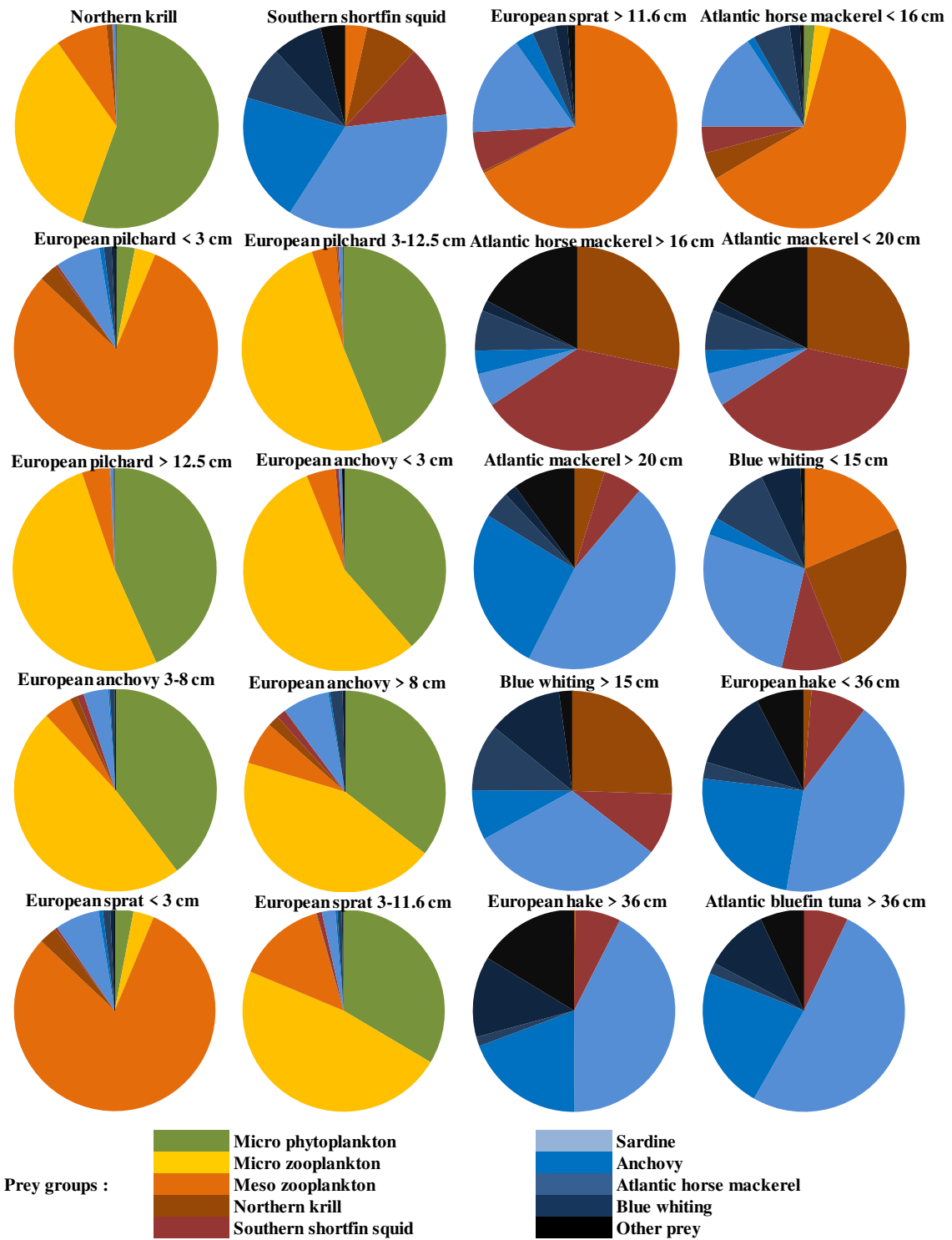
1270

1271

1272 **Fig. 6.**



1282



1284

1285

1286

1287 Fig. 8.

1288

1289

1290

1291

1292

1293

1294

1295

1296

1297

1298

1299

1300

1301

1302

1303

1304

1305

1306

1307

1308

1309

1310

1311

1312

1313

TROPIC  
LEVELS  
(TL)

4

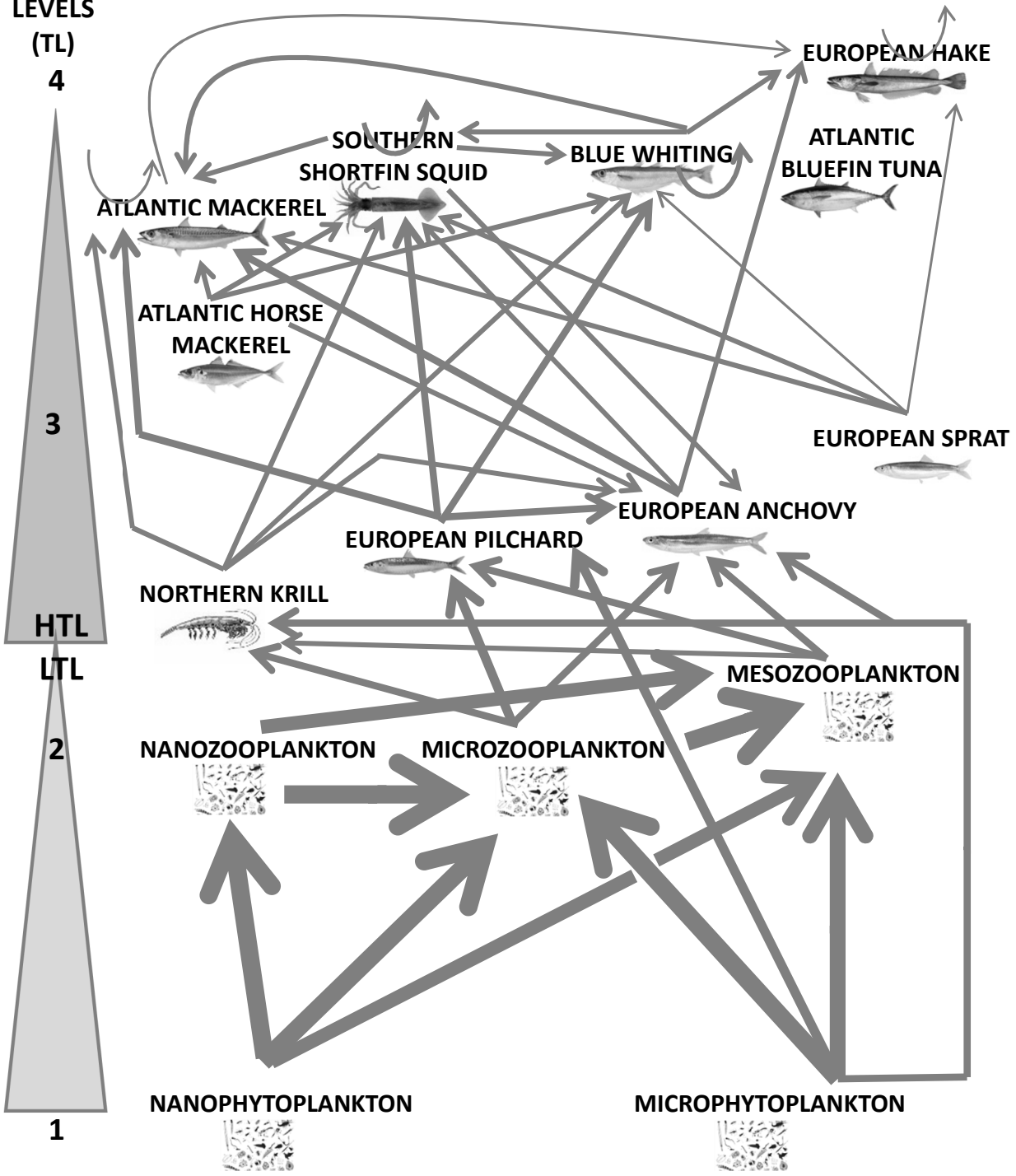
3

HTL

LTL

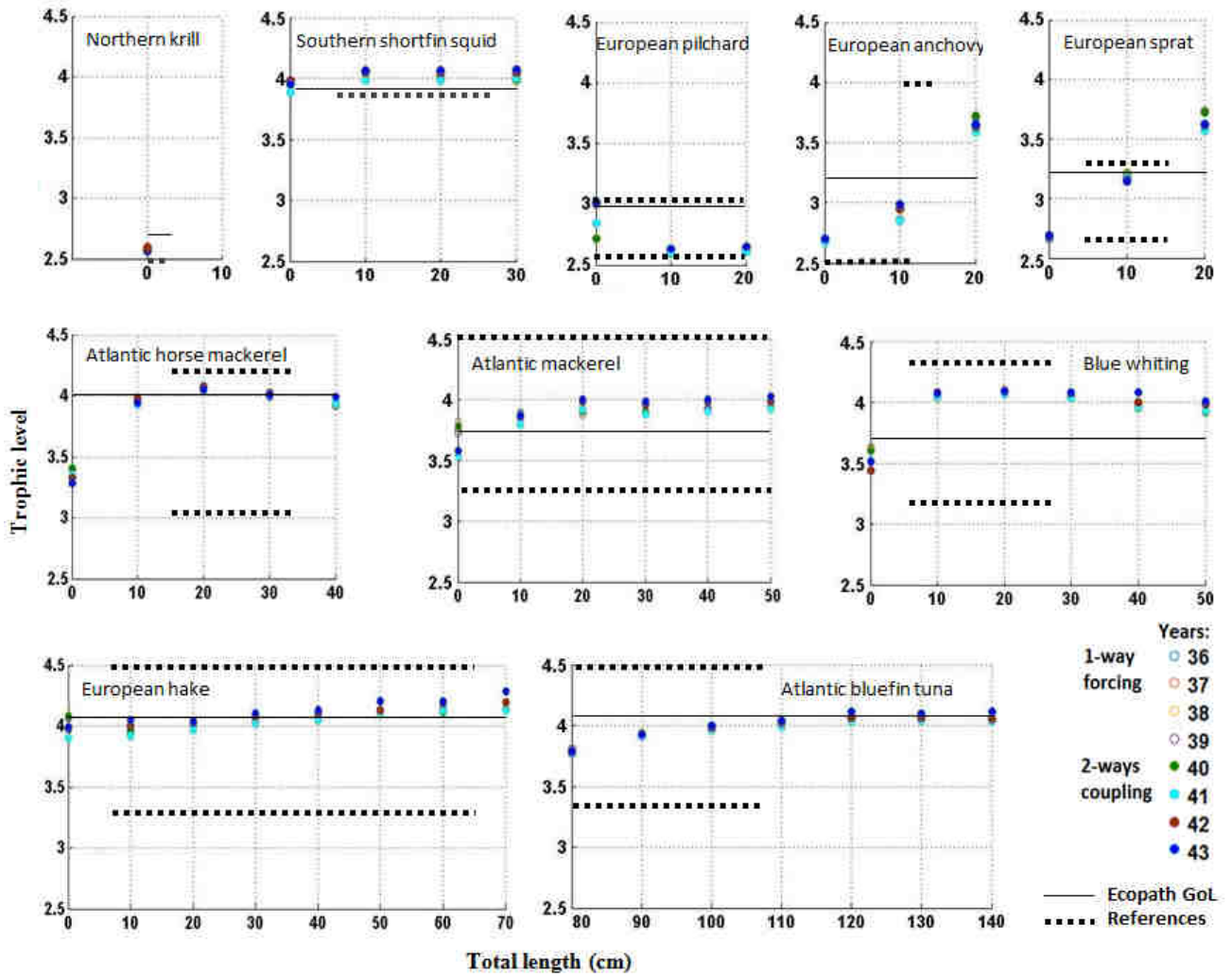
2

1



$\blacktriangleright >10^8$  ;  $\blacktriangleright 10^7 - 10^8$  ;  $\blacktriangleright 10^6 - 10^7$  ;  $\blacktriangleright 10^4 - 10^5$  ;  $\blacktriangleright 10^3 - 10^4$  ;  $\blacktriangleright 10^2 - 10^3$  ;  $\blacktriangleright 10 - 10^2 \text{ tons } y^{-1}$

1314 Fig. 9.



1315